F6.
⑫

SYSTEMS, SCIENCE AND SOFTWARE

AD A030795

EXPLOSION SOURCE MODELING, SEISMIC WAVEFORM PREDICTION AND YIELD VERIFICATION RESEARCH

T. C. Bache
T. G. Barker
J. T. Cherry
N. Rimer
J. M. Savino

Quarterly Technical Report

For Period February 1, 1976 - April 30, 1976

The views and conclusions contained in this
document are those of the authors and should
not be interpreted as necessarily represent-
ing the official policies, either expressed
or implied, of the Advanced Research Projects
Agency, the Air Force Technical Applications
Center, or the U.S. Government.

May 1976

AFTAC Project Authorization No. VELA T/6712/B/ETR

Program Code No. 6F10

Effective Date of Contract: May 1, 1975

Contract No. F08606-75-C-0045

Principal Investigator and Phone No.
        Dr. John M. Savino (714) 453-0060, Ext. 455

Project Scientist and Phone No.
        Dr. Ralph W. Alewine, III (202) 325-8484

S^3 Project No. 11014

REPORT DOCUMENTATION PAGE	READ INSTRUCTIONS BEFORE COMPLETING FORM

1. REPORT NUMBER	2. GOVT ACCESSION NO.	3. RECIPIENT'S CATALOG NUMBER

4. TITLE (and Subtitle)	5. TYPE OF REPORT & PERIOD COVERED
EXPLOSION SOURCE MODELING, SEISMIC WAVEFORM PREDICTION AND YIELD VERIFICATION RESEARCH	Quarterly Technical Report Feb. 1, 1976 – April 30, 1976
	6. PERFORMING ORG. REPORT NUMBER SSS-R-76-2924

7. AUTHOR(s)	8. CONTRACT OR GRANT NUMBER(s)
T. C. Bache, T. G. Barker, J. T. Cherry, N. Rimer and J. M. Savino	Contract No. F08606-75-C-0045

9. PERFORMING ORGANIZATION NAME AND ADDRESS	10. PROGRAM ELEMENT, PROJECT, TASK AREA & WORK UNIT NUMBERS
Systems, Science and Software P. O. Box 1620 La Jolla, CA 92038	Program Code No. 6F10 ARPA Order No. 2551

11. CONTROLLING OFFICE NAME AND ADDRESS	12. REPORT DATE
VELA Seismological Center 312 Montgomery Street Alexandria, VA 22314	May 1976
	13. NUMBER OF PAGES 54

14. MONITORING AGENCY NAME & ADDRESS(If different from Controlling Office)	15. SECURITY CLASS. (of this report)
	Unclassified
	15a. DECLASSIFICATION/DOWNGRADING SCHEDULE

16. DISTRIBUTION STATEMENT (of this Report)

Approved for public release; distribution unlimited.

17. DISTRIBUTION STATEMENT (of the abstract entered in Block 20, If different from Report)

18. SUPPLEMENTARY NOTES

19. KEY WORDS (Continue on reverse side if necessary and identify by block number)

Seismic Coupling, Earth Structure, Yield Determination, Explosive Source Modeling, Ground Motion Prediction

20. ABSTRACT (Continue on reverse side if necessary and identify by block number)

The theoretically computed and observed amplitudes of both the b and d (maximum) body wave phases for KASSERI agree to well within a factor of two at all of the five SDCS stations. Minor adjustments of the upper mantle model could improve the agreement at all the SDCS sites.

Computations of the effect of material strength on teleseismic body wave amplitudes indicate that the amplitude of the b phase increases with decreasing strength; the rate of increase being more rapid at lower levels of

DD FORM 1473 EDITION OF 1 NOV 65 IS OBSOLETE

material strength. An additional effect is that the apparent period of the
b phase increases rapidly with decreasing strength due to a shift in the corner
frequency of the source spectrum.

Further verification of the explosion source modeling code, SKIPPER, was
achieved by comparison of free field ground motion calculations and observa-
tions for the PILEDRIVER and GASBUGGY explosions. In the case of PILEDRIVER,
the exercise of a recently developed elastic wave propagation code verified
that the observed PILEDRIVER RDP was not affected by reflected waves from the
free surface or from layer interfaces in the source region.

Excellent free field ground motion measurements and material properties
data are available for the GASBUGGY explosion. The computed RDP, employing
these data, agrees quite well with the measured RDP, increasing our confidence
in the constitutive modeling of the explosion source and ultimately the tele-
seismic ground motion predictions based on these source calculations.

TABLE OF CONTENTS

I. SUMMARY

During the past several years, Systems, Science and Software (S³) personnel have been actively engaged in a comprehensive program involving computer modeling of the nonlinear processes that characterize underground nuclear explosions, propagation of the resultant stress wave through realistic earth structures and prediction of the ground motion recorded at teleseismic distances from an explosion. The objectives of the subject project are to employ these modeling and predictive capabilities in a systematic examination of the effects of variations in source and emplacement parameters on seismic signals from underground explosions, and to investigate methods for utilizing the general characteristics of seismic waveforms to obtain reliable yield estimates for explosions.

The technical phases necessary to accomplish the objectives of this project are as follows:

1. Conduct a systematic theoretical examination of material, source and emplacement parameters which affect yield-magnitude relationships and compare the theoretical predictions to actual observations.

2. Determine and express uncertainties of yield estimates in terms of uncertainties in gross earth structure, near source material properties, and local source and receiver structure.

Major accomplishments during the fourth three-month period of this project were realized in several different areas of research. Of particular importance was the exercise of our computational capabilities for the prediction and matching of teleseismically recorded body and surface waves from the recent Pahute Mesa explosion, KASSERI. Our objective

in this experiment was to model the near source (explosion) nonlinear processes, propagate the resultant stress waves through realistic earth structures and finally, generate synthetic seismograms for comparison with actual recordings obtained from five stations of the Special Data Collection System (SDCS) located at teleseismic distances from the Nevada Test Site (NTS). An important additional aspect of the waveform matching exercise for KASSERI is the comparison of ground motion for KASSERI with previous predictions for the MAST explosion (Barker, et al., 1976).

The theoretical and observed amplitudes of both the b(first half cycle) and d (maximum cycle within first 3 cycles) phases for KASSERI agree to well within a factor of two at all five SDCS stations. In general the fit is better for the b phase than for the d phase. A similar result was found for MAST as reported in Barker, et al. (1975). Minor adjustments of the upper mantle model could improve the agreement at all the SDCS stations; a step that should be taken before computing theoretical seismograms for additional events.

The relative scaling of the observed amplitudes for KASSERI and MAST at the SDCS sites is quite consistent (in terms of relative yields) except at RKON. It will be very difficult to explain the RKON anomaly with present computational techniques since the epicentral distance variation between events is only 0.1 degrees. Waveform similarities at the SDCS sites WH2YK, CPSO and HNME argue against attributing the apparent anomaly at RKON to near-source effects.

The effect of material strength on teleseismic body wave recordings, in particular the b phase, was examined. The amplitude of the b phase increases with decreasing strength, with the rate of increase being more rapid at lower levels of material strength. An additional effect is that the period of the b phase increases rapidly with decreasing

strength due to a shift in the corner frequency of the source spectrum.

A comparison of computed and observed free-field ground motion was made for the PILEDRIVER explosion, detonated in granite at NTS. The purpose of this experiment was to ascertain whether the observed free field recordings obtained at the time of the explosion were affected by waves reflected from the free surface or from interfaces between geologic layers. Comparison of near-field radial motions with different structures indicates that the observed recordings for Piledriver are unaffected by reflected waves and are appropriate choices for normalizing the source calculations.

A check of the constitutive modeling embodied in the SKIPPER code was made using free-field ground motion measurements for the GASBUGGY explosion detonated in New Mexico. Fairly complete material properties data were available for this event. The computed reduced displacement potential (RDP), incorporating all available information, is in excellent agreement with the observed RDP reported by Perret (1968). This result increases our confidence in source calculations used in predicting teleseismic waveforms generated by underground explosions.

II. INTRODUCTION

As stated in the previous section, the objectives of the subject research project are to utilize existing computational capabilities to examine the effects of various source and emplacement parameters on seismic signals from underground explosions, and to devise and evaluate methods for utilizing the general characteristics of seismic waveforms to obtain reliable estimates of explosion yields. In order to realize these objectives, activity on this program during the fourth three-month period of this contract concentrated in the following areas:

1. The prediction and matching of teleseismic body waves generated by the NTS explosion, KASSERI, and observed at the SDCS network. Comparison of the results with those for the MAST explosion.

2. Exercise of a recently developed elastic wave propagation code including both near- and far-field terms, to check for contamination of close-in ground motion recordings by reflected waves.

3. Verification of constitutive modeling using close-in free field ground motion data from the GASBUGGY explosion.

The plan of the remainder of this report is to present technical discussions of each of these three research areas, followed by a section summarizing the most important results obtained to date.

III.   TECHNICAL DISCUSSION

3.1   TELESEISMIC GROUND MOTION PREDICTIONS FOR THE KASSERI EXPLOSION

3.1.1   Calculation of the Equivalent Elastic Source

Coupling of the explosive energy into elastic waves was computed using the one-dimensional (spherically symmetric) finite difference code, SKIPPER. Description of the technique and the constitutive models may be found in Cherry, et al. (1975).

KASSERI was detonated in ash flow tuff at Area 20, Pahute Mesa. The working point was well below the water table. Standard measurements for density, grain density, overburden density, water content, saturation and P wave velocity were available. It should be noted that the P wave velocity was not measured but was estimated from events in similar media.

No material strength data were available. Therefore, we were forced to estimate the material strength from other information. A study of the effect of plausible strength variations on the seismic signal was carried out as part of the KASSERI investigation and will be discussed.

The equation of state table (pressure as a function of specific volume and specific internal energy) for the saturated tuff was generated using the TAMEOS scheme (Riney, et al., 1973). In this scheme grain density tuff is mixed with the appropriate amount of water, assuming pressure equilibrium between the mixture and its components. From the bulk modulus (K) obtained from the TAMEOS table at the overburden pressure and P wave velocity (α), the shear modulus is calculated from $\rho\alpha^2 = K + 4\mu/3$. The hydrostatic overburden pressure is obtained from the given depth of burial and overburden density.

5

All calculations used an effective stress law to account for the effect of pore fluid pressure on the stress state. The material was assumed to fail in tension; that is, a tension failure model was invoked if any principle stress became tensile.

Since no data were available on the shear strength of the KASSERI tuff or similar materials in Pahute Mesa, a series of calculations were made in which the material strength was varied. All other material properties required for the calculation (bulk density, grain density, percent water by weight, percent air-filled voids, P wave velocity, overburden pressure, bulk modulus of overburden, shear modulus) were held fixed at the given values.

Previous calculations for Pahute Mesa rhyolite (Cherry, et al., 1975; Barker, et al., 1976) used a laboratory determined failure envelope for granite. Taking this as a starting point, we then perturbed the failure envelope to values that might be appropriate for the almost certainly weaker tuff. The parameters controlling the failure envelope are summarized in Table 3.1 for the four calculations completed. The parameters in the table are defined as follows:

$$Y(P,e) = \left(1 - \frac{e}{e_m}\right)\left[Y_0 + Y_m \frac{\overline{P}}{P_m}\left(2 - \frac{\overline{P}}{P_m}\right)\right] , \quad \overline{P} < P_m, \ e < e_m,$$

$$= \left(1 - \frac{e}{e_m}\right)\left(Y_0 + Y_m\right) , \quad \overline{P} \geq P_m, \ e < e_m, \quad\quad (3.1)$$

$$= 0, \ e \geq e_m,$$

$$\overline{P} = P - \frac{1}{2} \frac{\sqrt{J_3'}}{2}$$

where J_3' is the third deviatoric stress invariant, P is the pressure including the overburden and e is the specific

6

TABLE 3.1

FAILURE ENVELOPES FOR KASSERI CALCULATIONS

Calculation	Y_0 (kbar)	Y_m (kbar)	P_m (kbar)	e_m (10^{10}ergs/cm)
146	0.1	7.9	9.0	2.0
147	0.3	7.7	9.0	2.0
148	0.15	3.85	9.0	2.0
149	0.075	1.925	9.0	2.0

internal energy. The Y is the maximum stress difference or twice the maximum shear stress. The meaning of these parameters is indicated schematically in Figure 3.1.

From the table we see that only the parameters Y_0 and Y_m were changed from calculation to calculation. The granite failure surface was used for 147. Calculations 148 and 149 are for the same failure surface with the strength cut by a factor of 2 and a factor of 4. Calculation 146 was done to see the effect of changing the shape of the failure surface while leaving the high pressure strength ($Y_0 + Y_m$) unchanged.

The amplitude of the reduced velocity potential, $|\hat{\Psi}(\omega)|$, is plotted in Figure 3.2 for the four sources of Table 3.1. Also shown is the rhyolite source used for the MAST calculations reported by Barker, et al. (1976). The $\hat{\Psi}(\omega)$ is essentially the far-field displacement spectrum. In fact,

$$m_b \approx \log \alpha \hat{\Psi} \ (1 \ Hz),$$

$$(3.2)$$

$$M_s \approx \log \mu \hat{\Psi} \ (0.05 \ Hz),$$

as has been demonstrated theoretically in a number of past S^3 reports (e.g., Bache, et al., 1975a, 1975b).

In the following section we will be discussing the teleseismic body wave that results from the source functions of Figure 3.2. The surface waves will be discussed in a forthcoming technical report. However, we can draw some conclusions from the character of the source spectra alone. In Table 3.2 are summarized the main characteristics of the spectra: The zero frequency limit (Ψ_∞), the peak value ($|\hat{\Psi}|$), the ratio of peak to zero freqeuncy limit, the peak frequency
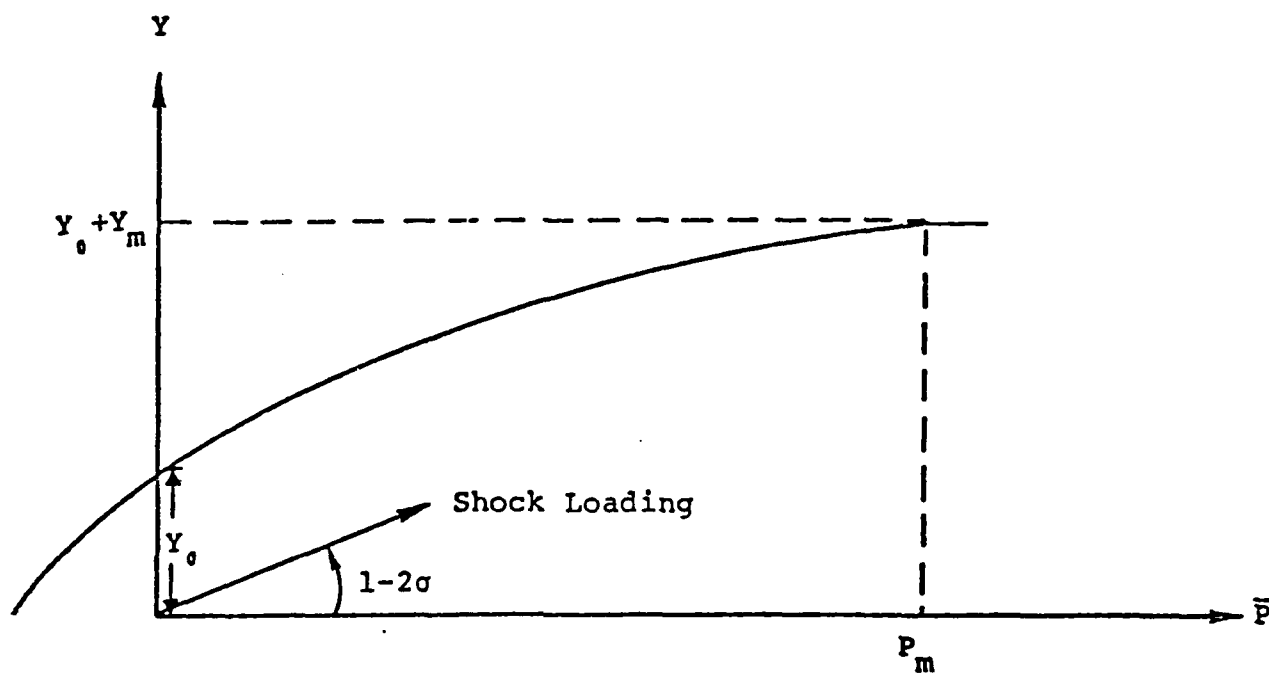
8

Figure 3.1. Assumed relationship between the material strength
(Y) and the hydrodynamic component of stress ($\bar{P}$)
for small e/e_m. When $\bar{P}$ is used for the abcissa
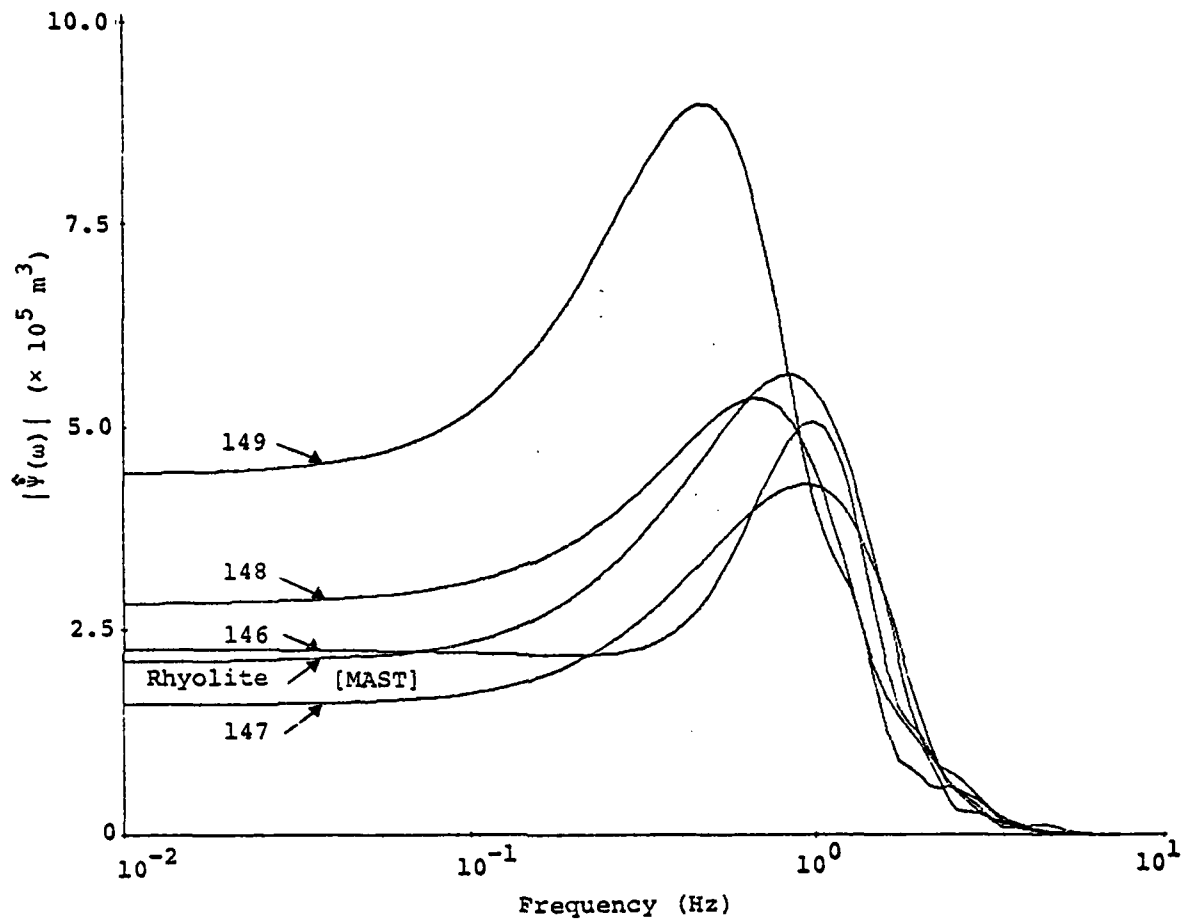the shock loading path has a slope of $1-2\sigma$.

Figure 3.2. The source function amplitudes for the tuff sources of Table 3.1 and the rhyolite source for MAST. The source functions are all scaled to 1000 kt.

TABLE 3.2

SOURCE FUNCTION CHARACTERISTICS AT 1000 KT

Source	Ψ_∞ ($\times 10^5 m^3$)	$|\hat{\psi}_p|$ ($\times 10^5 m^3$)	$\dfrac{|\hat{\psi}_p|}{\Psi_\infty}$	f_p (Hz)	Peak Width (Hz)
146	2.25	5.05	2.24	0.96	0.70
147	1.60	4.30	2.69	0.93	1.18
148	2.90	5.35	1.84	0.67	0.76
149	4.40	8.95	2.03	0.47	0.54
MAST	2.10	5.70	2.71	0.84	1.00

(f_p) and the width of the peak at the amplitude halfway between Ψ_∞ and $|\hat{\Psi}|$. Comparing 146 and 147, we see that the low strength portion of the strength curve significantly narrows the peak while having a relatively minor effect elsewhere. Comparing 147, 148, 149, as the strength is decreased the spectrum gets larger. Also, the peak becomes narrower and moves to lower frequencies. The MAST source exhibits behavior between that of 147 and 148.

For MAST and KASSERI the important parameters controlling the teleseismic coupling are α = 4.2 km/sec, μ = 169 kbar for MAST and α = 3.1 km/sec and μ = 90 kbar for KASSERI. These values together with the source functions in Figure 3.2 and Table 3.2 give a first estimate of the relative size of the body and surface waves for these two events. Detailed comparison of theoretical and actual seismograms is made in the following section.

3.1.2 Computational Procedure for Ground Motion Predictions

In our report on MAST (Barker, et al., 1976) we outlined the procedure followed to predict the short and long period seismograms at selected SDCS stations. For KASSERI we follow the same procedure. Using the best available information for the rock properties at the working point, we compute an equivalent elastic source (RDP) for the explosion. This was discussed in the previous section. We also construct a layered earth model for the source vicinity from available information. The remainder of the calculation is identical for the two events.

In this section we discuss the theoretical body waves for KASSERI and compare them to observations. For comparison we also include the MAST results from Barker, et al. (1976).

3.1.3 Earth Models for Theoretical Body Wave Calculations

The source region crustal structure for KASSERI is tabulated in Table 3.3. The top two kilometers of this structure are different from that for MAST; below that the two structures were taken to be the same.

Modeling of the remainder of the travel path is as described in our MAST report. For the structure at the receiver an average crustal model having little effect on the seismograms was used at all stations. This model, which is tabluated in Table 3.4, was chosen for the lack of any better information. For the upper mantle we chose a slightly modified version of the Helmberger and Wiggins (1971) model HWNE. The P wave-depth profile for this model, together with the revised version, HWNE-3, is shown in Figure 3.3.

The other factor to be selected is the parameter T/Q which characterizes the attenuation along the path. Results will be shown for two values of T/Q = 1.05 and 0.95.

3.1.4 Comparison of Theoretical and Observed Short Period Recordings

We chose the source 148 (Figure 3.2) to be the most appropriate for the KASSERI event. In the following section we will compare the seismograms for this source to those obtained using the other three sources with different failure envelopes, but for the comparison of theory and observations made here, 148 is the source. Note that this is the source with strength $(Y_0 + Y_m)$ half that of granite

The wave form comparisons are shown in Figure 3.4. For each of the five SDCS stations at which theoretical seismograms were made, we show first the comparison of theory and observations for MAST from Barker, et al. (1976), then the comparison for KASSERI. Comparing seismograms for the two events at each station, we can see how much the signals vary theoretically and as observed.

TABLE 3.3

SOURCE REGION CRUSTAL STRUCTURE FOR KASSERI

Depth	Thickness (km)	α (km/sec)	β (km/sec)	ρ (g/cm^3)
0.11	0.11	3.05	1.07	2.10
0.33	0.22	2.75	1.50	1.85
0.42	0.09	3.00	1.70	2.05
0.50	0.08	4.40	2.40	2.15
0.91	0.41	2.88	1.60	1.95
1.50	0.59	3.11	1.80	2.20
2.10	0.60	4.30	2.40	2.60
6.00	3.90	4.70	2.60	2.60
12.00	6.00	5.40	2.70	2.70
20.00	8.00	6.00	3.50	2.80

TABLE 3.4

RECEIVER REGION CRUSTAL STRUCTURE

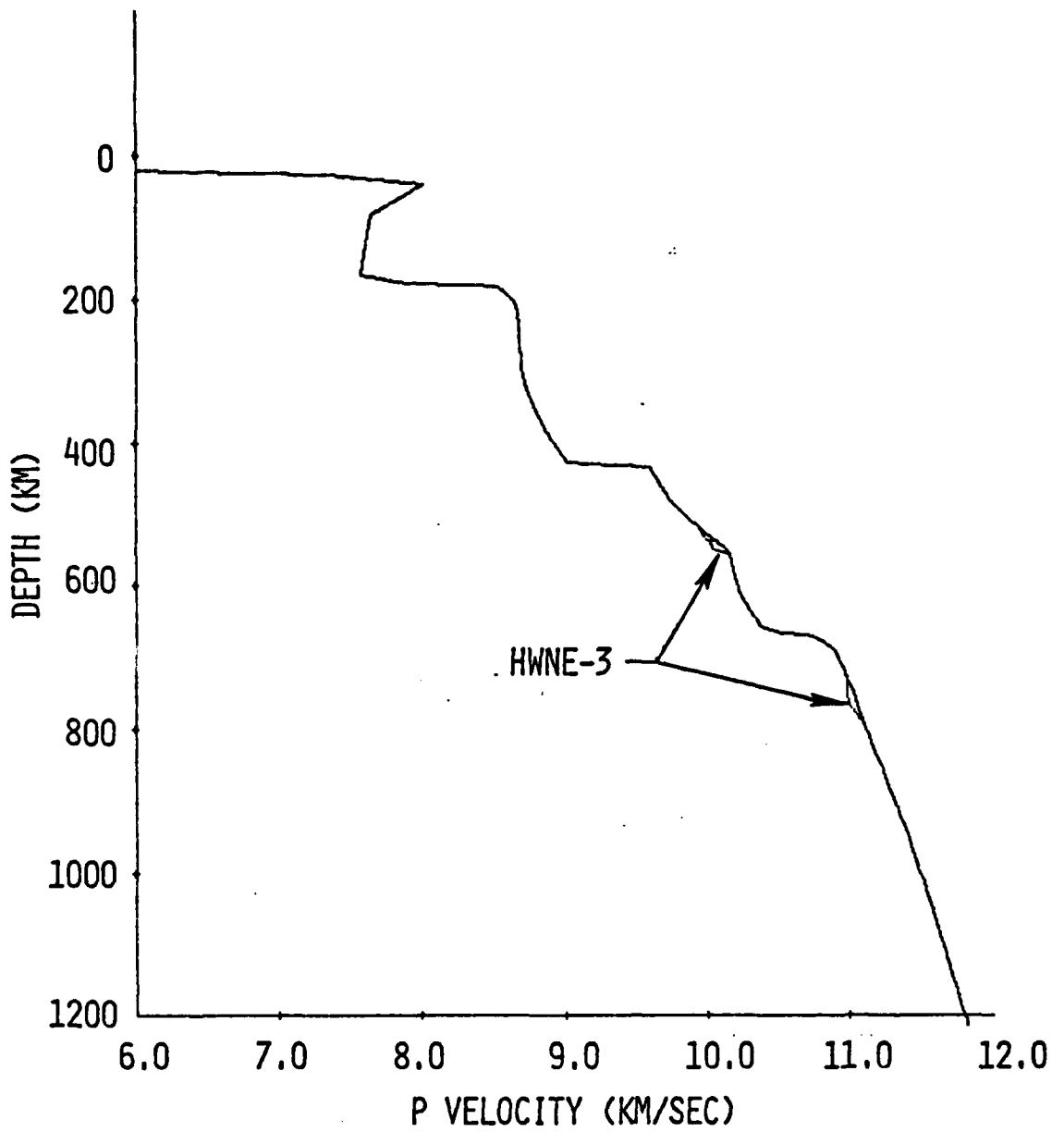| Depth (km)	Thickness (km)	α (km/sec)	β (km/sec)	ρ (gm/cm^3)
2.58	2.58	3.67	2.31	2.40
4.84	2.26	5.42	3.27	2.60
11.61	6.77	5.80	3.45	2.60
20.00	8.39	6.00	3.50	0.80

Figure 3.3. P velocity versus depth for the upper mantle model
HWNE-3. This model is a slightly modified version
of HWNE (Helmberger and Wiggins, 1971) with the
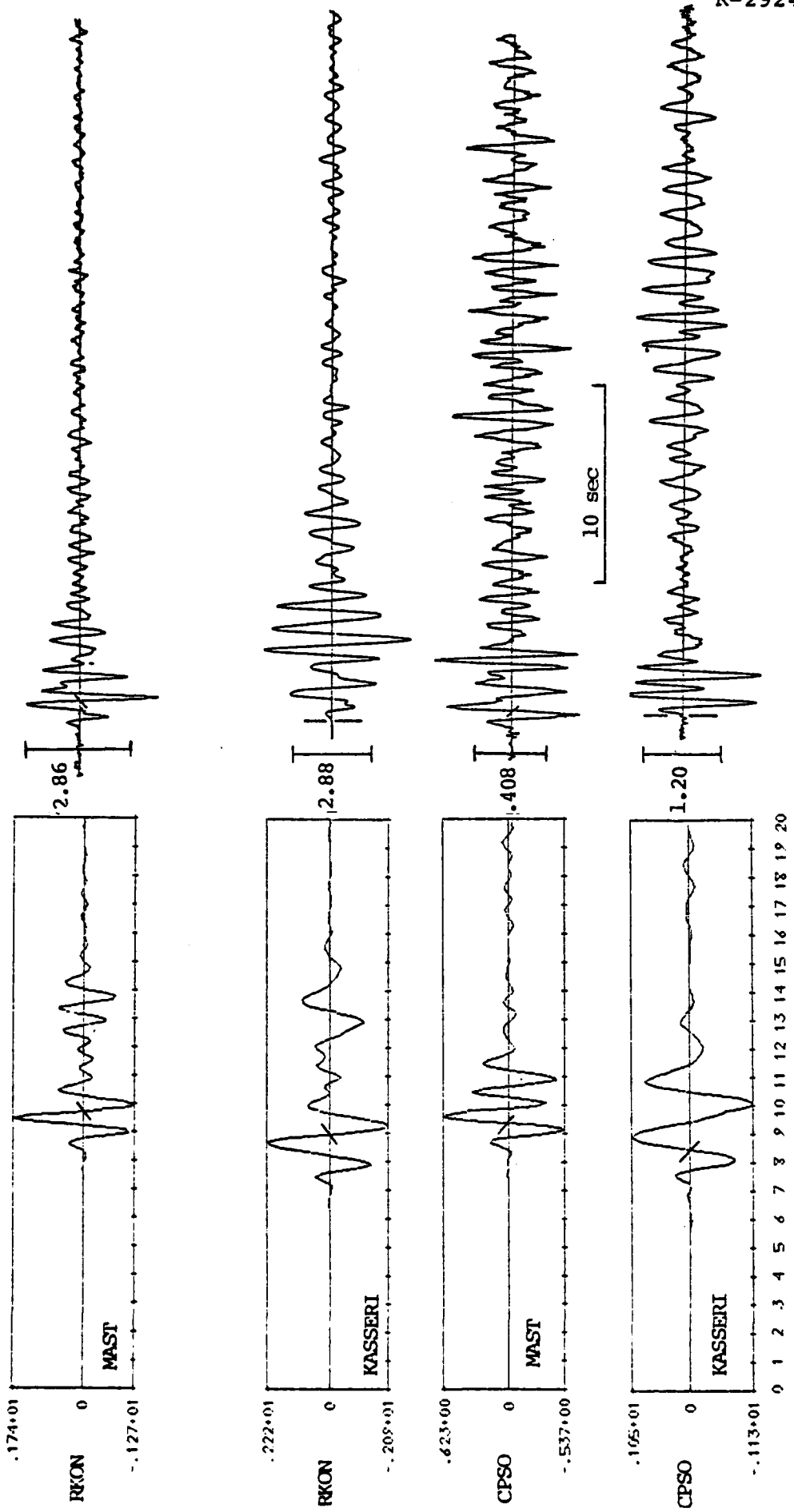differences as indicated in the figure.

16

Figure 3.4. Comparison of synthetic (left) and observed short period vertical component seismograms at five SDCS stations for the events MAST and KASSERI. The amplitude at 1 Hz is indicated at the left on each record. The bars show the cycle at which the maximum or "d" amplitude measurements were made.

TIME (SEC)

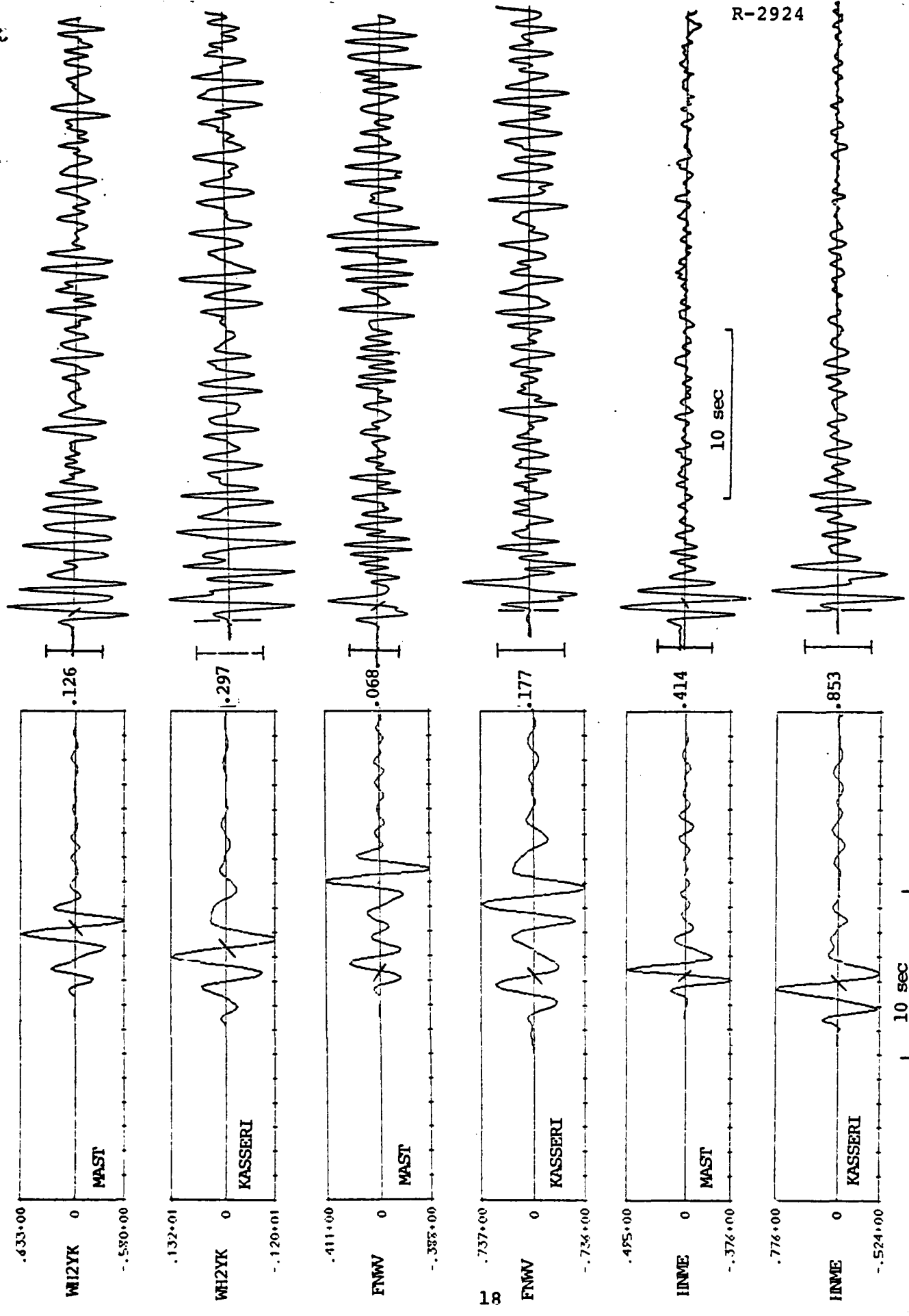0 1 2 3 4 5 6 7 8 9 10 11 12 13 14 15 16 17 18 19 20

R-2924

Figure 3.4. (Continued)

The difference between the two events are in the source material, as mentioned, and in the yield which is about twice as large for KASSERI as MAST. The distance to the stations of Figure 3.4 is approximately 10 km greater for KASSERI than MAST, a seemingly trivial change. The depths are H = 0.91 km for MAST and H = 1.26 km for KASSERI. The theoretical P-pP lag time is then approximately 0.50 seconds for MAST and 0.82 seconds for KASSERI.

Examining the observations, we see an extraordinary change in the shape of the RKON recording between the two events. At the other stations the difference are much less pronounced. In fact, at the other stations one could argue that the waveform differences are primarily the result of the change in P-pP lag time.

The theoretical seismograms were computed with T/Q = 0.95. We also computed the same stations with T/Q = 1.05 and will be discussing measurements made from both sets. For a visual comparison as in Figure 3.4, the difference between the two is hardly apparent. At each station the instrument response was taken from calibration data provided by the Project Officer. The calibration was done just prior to MAST but was used for KASSERI as well.

Regarding the comparison of theoretical and observed waveforms, we can only make the same comments as in the MAST report. The phenomena that seems to dominate the response at the nearer four stations is not accurately represented in our models. Our theoretical signals also fail to include much of the high frequency energy that appears after the first few seconds of the record.

The important fact is that it does appear that we have properly included the factors controlling the amplitude of the b phase, the first cycle on the record. This phase is least affected by phenomena not related to the explosion coupling into elastic waves – the feature presumably most

19

indicative of explosion yield. Evaluation of the comparison should rely most heavily on the b phase data.

The comparison between theoretical and observed amplitudes from the seismograms of Figure 3.4 is shown in Figures 3.5 and 3.6. The data in Figure 3.5 is for the "b" phase; that in Figure 3.6 is for the maximum amplitude in the first three cycles, the "d" phase. Along with the plotted b and d amplitudes, the periods of the cycles at which these were measured appear on the figures.

With regard to the data of Figures 3.5 and 3.6 there are two important observations to be made. First, the amplitude and period of the "apparent ground motion" is dependent on the characteristics of the recording instrument. Unfortunately, it is not necessarily true that a plot of actual versus theoretical "true ground motion" amplitudes would have the same appearance as the plots of Figures 3.5 and 3.6. This is because the instrument correction to true ground motion, as conventionally used, has an erratic effect. This subject is discussed in some detail in Appendix A where we show the results of the following numerical experiment: (1) The theoretically computed ground motion for KASSERI at HNME is filtered by six different short period instruments; one being specified by LRSM nominal instrument response curves and the others specified by calibration data provided by the Project Officer for the five SDCS stations. (2) Synthetic seismograms were computed. (3) Amplitudes were measured in the conventional way; since the entire process is done digitally, the errors in the measurement of amplitude and apparent period can be reduced to nearly vanishing.

The results of the numerical experiment outlined above is somewhat surprising. The apparent period is used to determine an instrument correction to what we shall call "apparent ground motion". Even though the actual ground motion is identical, this apparent ground motion varies over a large
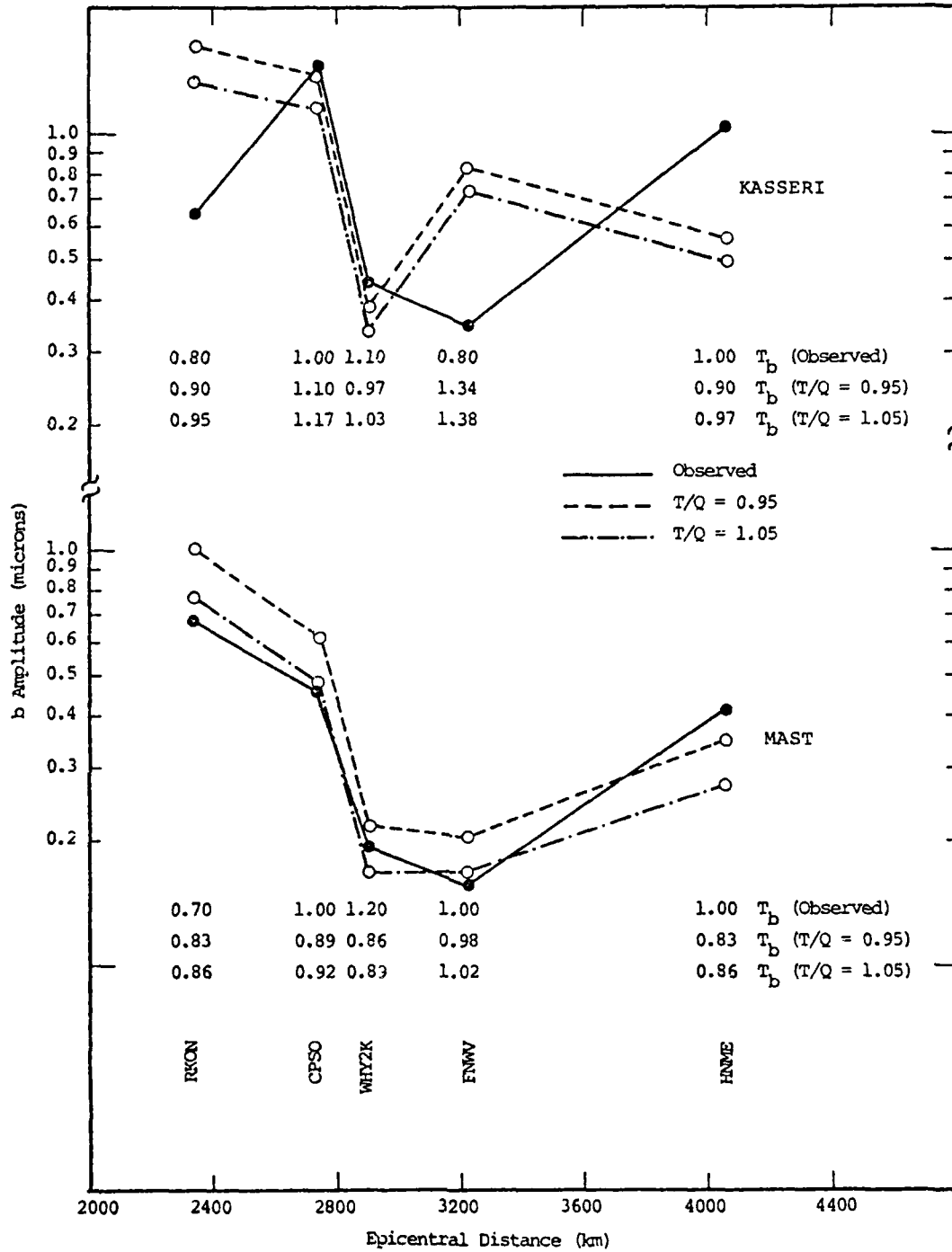
Figure 3.5. Comparison of theoretical and observed b ampli-
tudes for MAST and KASSERI at five SDCS stations.
Seismograms were computed for two values of T/Q
as indicated. The KASSERI source function is
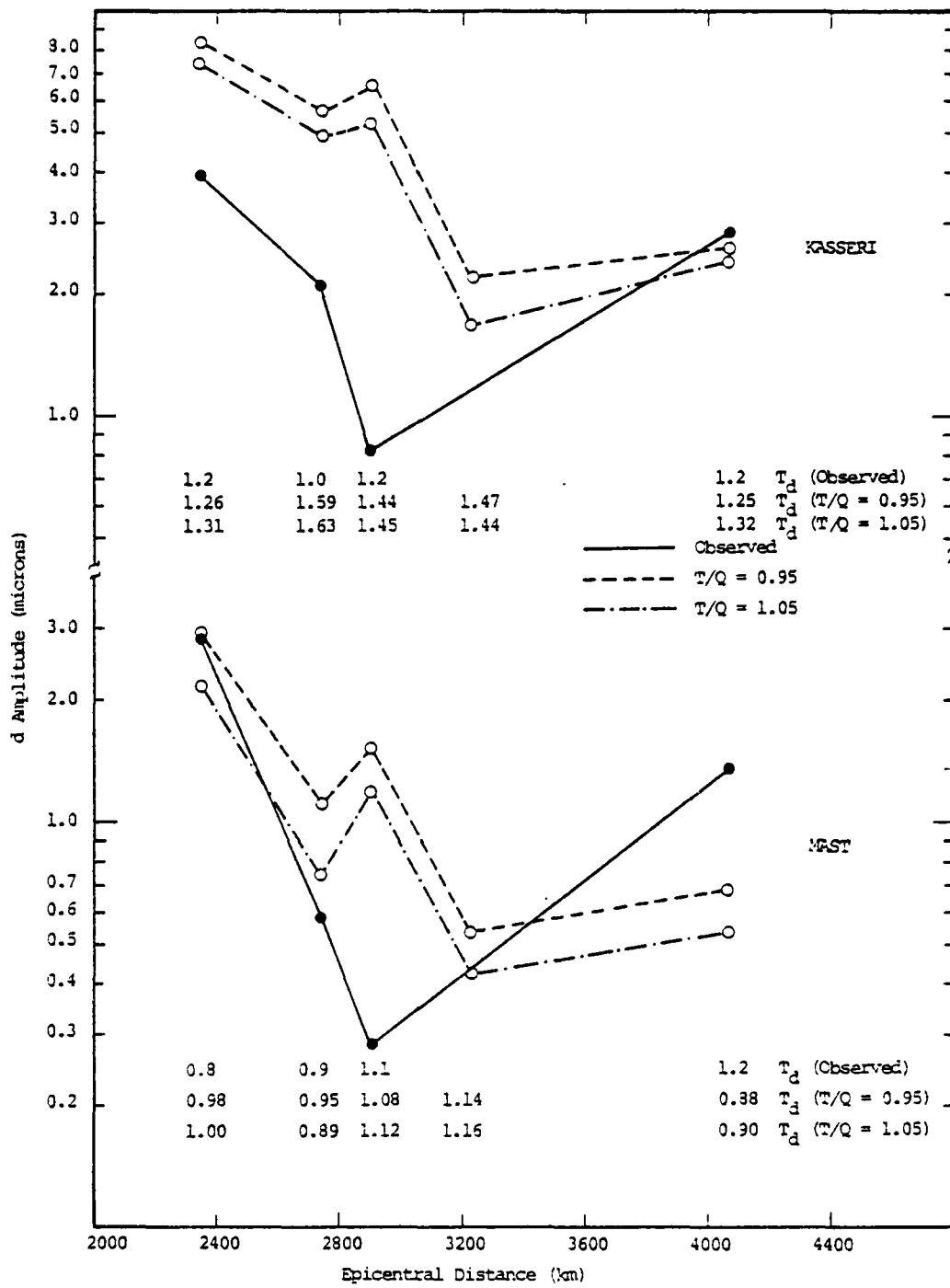denoted 148 and the upper mantle model is HWNE-3.

Figure 3.6. Comparison of theoretical and observed d amplitudes for MAST and KASSERI.

22

range; as much as a factor of two! It turns out that the discrepancy would be much reduced if no instrument correction were applied.

The second point to be made is closely related to the first made above. We find that we must know the instrument response quite accurately to be able to compute theoretical seismograms that are comparable to the actual observations. But how well do we know this response? How carefully are the instruments calibrated? At present we have no way of making a judgment.

The "observed" data plotted in Figures 3.5 and 3.6 are based on amplitude and period measurements made at S^3. Once again, the instrument correction problem arises. We believe that the amplitudes appearing in the SDCS Event Reports (No. 18 for MAST and No. 41 for KASSERI) were corrected for instrument response using LRSM nominal curves. We used the specific instrument curves provided by the Project Officer. These were based on calibrations carried out just before MAST and we can only hope that they remained valid for KASSERI - both for the observations and for synthesized seismograms.

From the comparison of Figures 3.5 and 3.6 we draw the following conclusions:

- The scaling of observed amplitudes between the two events is quite consistent except for RKON. We previously pointed out the marked disimilarity in waveforms at RKON for these two events.

- The match between theoretical and observed amplitudes is about the same for the two events. The exceptional stations are RKON and FNWV. It will be very difficult to explain the RKON anomaly with present techniques since the epicentral distance variation between events is only 0.1

23

degrees. Wavefore similarities at WHY2K, CPSO and HNME discourage attempts to attribute the anomaly to near-source effects. Even in our theoretical model the interference pattern at FNWV is enough to make the b amplitude behave erratically as we see by comparing results for the two events. However, it is unlikely that plane layered models of the crustal structures beneath FNWV would permit a very accurate duplication of observed records at this station.

● The scaling between the two computed source functions seems to be approximately correct. Perhaps the MAST source is relatively larger than that for KASSERI.

● Differences between theoretical and observed amplitudes are less than a factor of two nearly everywhere. Minor adjustments of the upper mantle model could improve the agreement at all these stations.

● Changing T/Q from 0.95 to 1.05 increases the period of the phase measured by $\approx$ 0.03 - 0.07 seconds. The increase in amplitude is 15 - 25 percent.

● The periods of the b phase measured off the synthetic seismograms generally agree with the observations. If anything, they may be a little too short on the average. For the d phase the theoretical periods are clearly too long.

3.1.5 The Effect of Material Strength on Teleseismic Body-wave Recordings

The KASSERI calculations of the previous section were done with the source 148. How much different would the results be if we had used one of the other three sources of

Table 3.1? We compare the four sources, which vary only in
the specification of the material strength, by computing
seismograms for station HNME with T/Q = 1.05. The seismo-
grams are shown in Figure 3.7. The b amplitudes were mea-
sured from these records and are plotted versus the limiting
material strength $(Y_0 + Y_m)$ in Figure 3.8. Also shown is the
period of the b measurement. Since these seismograms were
computed with the LRSM normal instrument response, direct
comparison with the KASSERI observations is not possible.
However, in Appendix A, Table A.2, we show that the HMNE
specific instrument gives a b phase amplitude that is 0.46
as large and a period that is 0.19 seconds shorter.

The b phase data of Figure 3.8 is consistent with our
discussion of the spectral characteristics of the four source
functions (Figure 3.2) given in Section 3.1.1. The amplitude
increases with decreasing strength and the rate of increase
is more rapid at lower strength. The period of the waveform
increases rapidly with decreasing strength due to the shift
in corner frequency. For b amplitude there is essentially
no difference between the two sources (146 and 147) that have
the same ultimate strength as granite, even though the shape
of the yield surface is different.

In the previous section we saw that 148 was reasonably
successful. If in error, one would think 148 to be too low
in amplitude and to have too little energy (relatively) in
the high frequencies. We see in Figure 3.8 that improvements
in these two features require adjustments to the strength in
opposite directions. Also, a strength of about half that of
granite seems reasonable. If we are satisfied with the MAST
source which scales to the MAST source in a manner consistent
with the observations is also required. Source 148 seems to
fulfill this criterion fairly well. For all these reasons
mentioned above, we selected the source 148 as being most
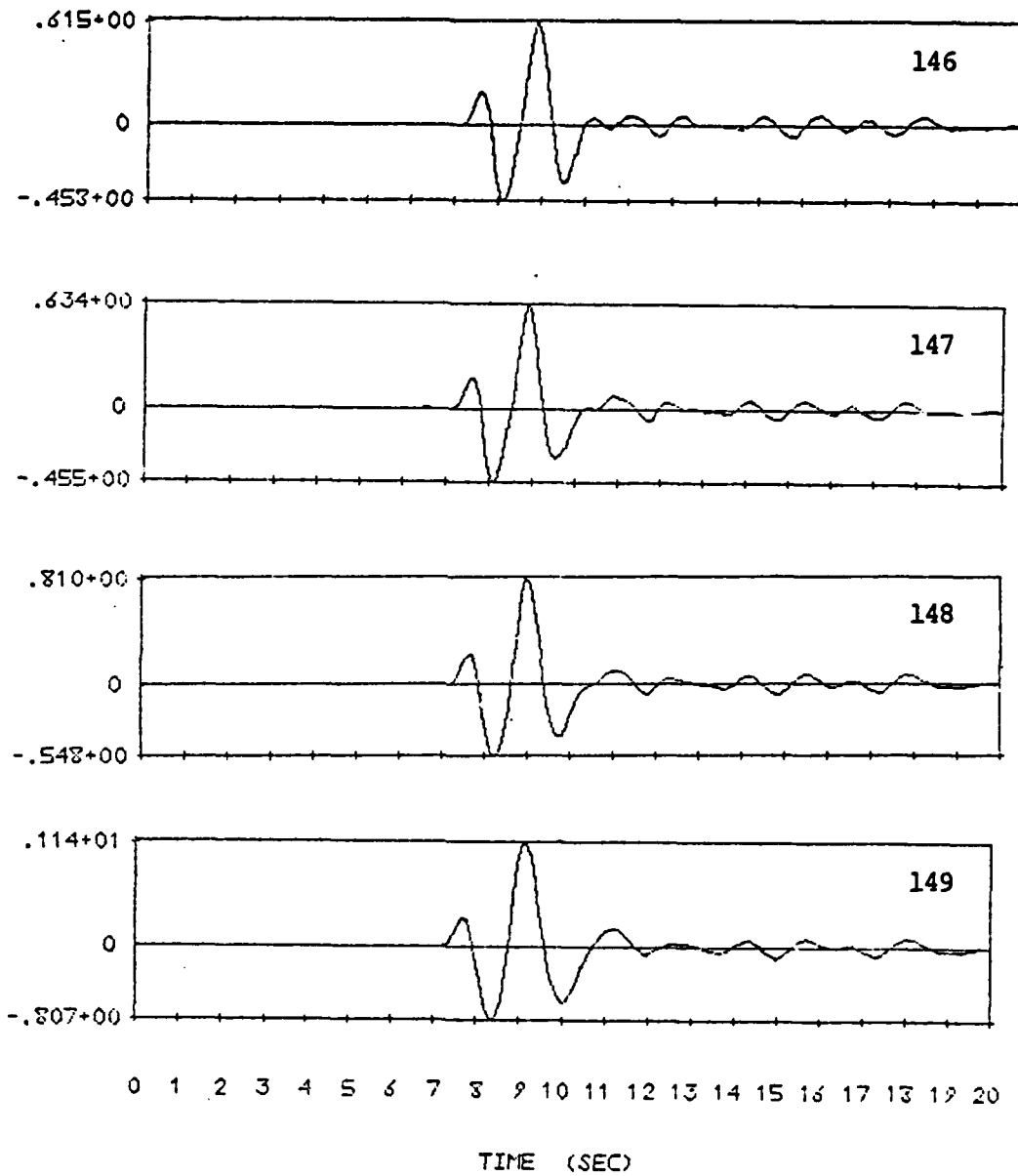representative of KASSERI. The data of Figure 3.8 are quite

Figure 3.7. Synthetic seismograms at HMNE for the four tuff source functions of Table 3.1. The parameters of the calculation are the same as for Figure 3.4 except T/Q = 1.05 and thw LRSM instrument response was used.

149
(Y_m = 1.925)

2000

1800

T = 1.32

1600

1400

b Amplitude (mµ)

1200

148
(Y_m = 3.85)

1000

T = 1.15

800

146
(Y_m = 7.9)
T = 0.98

600

147
(Y_m = 7.7)
T = 0.96

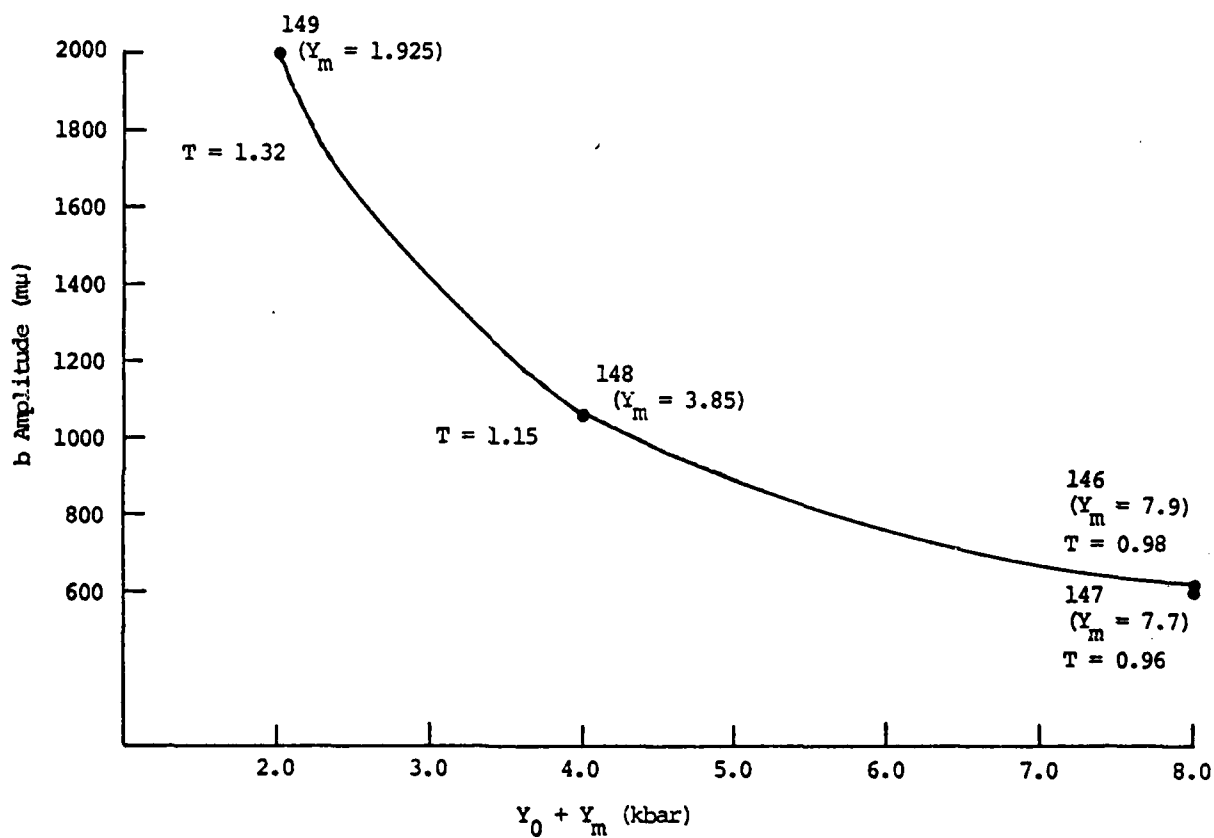2.0   3.0   4.0   5.0   6.0   7.0   8.0

$Y_0 + Y_m$ (kbar)

Figure 3.8. The b phase measurements for theoretical seismo-
grams at HNME computed with four source functions.
The source functions represent KASSERI tuff with
four different estimates of material strength.
The instrument response was the LRSM nominal.

27

important as an indication of the effect of erroneous esti-
mates of material strength.

3.2   PILEDRIVER GROUND MOTION CALCULATIONS

3.2.1 Introduction

An elastic wave propagation code, based on generalized
ray theory, was recently developed. This computational code
capability enables us to synthesize the complete elastic wave
field propagating from an explosive source, including both
near- and far-field terms. An immediate application of this
code was made to the PILEDRIVER explosion, detonated in
granite at NTS.

In fitting calculated ground motions produced by the
PILEDRIVER RDP to the observed free-field recordings, it was
assumed (Cherry, et al., 1975) that the observed data were
relatively unaffected by waves reflected from the free sur-
face or from interfaces between geologic layers. The RDP
is, of course, one-dimensional so that such effects were not
included in the calculations. The purpose of the calculation
to be described below was to ascertain the validity of this
assumption. The results of this calculation follow a brief
description of the wave propagation code.

3.2.2 Description of Wave Propagation Code

The calculation of the RDP is made with the 1-D SKIPPER
code. This code assumes that the highly nonlinear process in
which the explosion energy is coupled into shock waves ar.
then into elastic stress waves is a one-dimensional process.
Included is the assumption that local heterogeneities do not
significantly disturb the spherical symmetry of the radiation.
It should be noted that two-dimensional sources may be treated
in an analogous way (e.g., Bache and Harkrider, 1976; Cherry,
et al., 1976).

28

The use of elastic wave propagation techniques is justified if the following assumptions are correct: For the wavelengths of interest, the interfaces between layers are plane parallel. (This assumption may be relaxed to allow non-parallel layers.) Although we consider reflections and transmissions where the material response is clearly in the nonlinear source region, we assume that the interface behavior is not too different from that for elastic waves so that elastic reflection and transmission coefficients may be used. The analytical propagation technique is exact insofar as elastic wave propagation in layered media is concerned. Thus, all frequencies are propagated accurately in the layered medium. It is possible to include an anelastic attenuation factor in the analytical propagation theory (this is presently being implemented), but no such factor was included in the calculations discussed here. Of course, the explosion wave is strongly attenuated in the 1-D nonlinear calculation from which the RDP is obtained.

The elastic wave propagation program used here is based on generalized ray theory. A brief description of its salient features follows. A ray theory is based on the fact that the response of an elastic system can be represented as a series, each term of which being identified as the contribution of a particular ray. A ray is characterized by a ray path, which is a description of the number of traverses the ray makes across the layers, and the mode (P or S wave) of the traverses. For example, for a source and receiver above an interface, the solution is composed of three rays: The direct ray, the ray which travels to the interface as a P wave and returns as a P wave, and the ray which returns from the interface as an S wave. The solution is formulated in a way described by several authors (e.g., Helmberger, 1968).

It has been shown that the response u (a component of displacement, velocity, or stress) at the cylindrical

coordinates (x,z,θ) and time t, due to a source at the origin can be written as:

$$u(x,z,\theta;t) = \psi(t) * \sum_{j=1}^{N} \int_{t_{0j}}^{t} f(p_j,\tau)S(p_j)R(p_j)T_j(p_j)C(p_j)d\tau$$

Here, j is the ray index, and N indicates the number of rays to be included. The integration starts at the arrival time t_{0j}. The complex parameter p_j is chosen to make the imaginary part of τ vanish, where

$$\tau = p_j x + \sum_{\ell=1}^{L} \left(\frac{1}{v_\ell^2} - p_j\right)^{1/2} h_\ell, \tag{3.4}$$

and V_ℓ and L_ℓ are the layer velocities and thicknesses. At the arrival time, $p_j(t_{0j})$ is known as the ray parameter in geometrical optics. The function $S(p_j)$ specifies the source type (e.g., explosive), $R(p_j)$ specifies whether the incoming wave at the receiver is shear or compressional, and $C(p_j)$ determines the quantity (e.g., vertical displacement) being computed. The effect of the interfaces is included in the product of the reflection and transmission coefficients $T_j(p_j)$, while $f(p_j,\tau)$ is a kernal common to all these calculations. The RDP $\psi(t)$, is the time history of the source and $*$ denotes convolution.

The integration (3.3) is performed for each ray along the complex path set by (3.4), with the integrands computed on a finer spacing near t_0 where they are changing fastest. The ray responses are then added together and convolved with ψ to yield the final result. Classical (far-field) seismology makes approximations to (3.3), so that the integration need not be performed. This is the technique by which most "ray theory" calculations have been done. These approximations generally require that the periods of interest be much smaller

30

than the travel time, or equivalently, that the receiver be many wavelengths from the source. For the calculations done for this report, the situation is reversed, making it necessary to fully evaluate (3.3).

In evaluating Eq. (3.3), we must add N rays together to form the response. For most layered geometries, N is infinite. For example, when a source and receiver are in a sandwiched layer, there are an infinite number of ray paths corresponding to all the internal reflections in the layer. However, with each reflection the rays are attenuated because they travel farther and because they leak energy out of the layer. In practice, the rays which are important for a particular problem are easily determined. The calculation is inexpensive to run so that if one is in doubt about the inclusion of a set of rays, numerical experiments can be cheaply done to resolve that doubt.

Note that the RDP affects the solution via a convolution. Thus, the RDP and the layered responses are computed independently, and finally convolved.

3.2.3 Results of Source Calculation

To check whether reflected waves from the vertical layering, in particular the free surface, could have influenced free-field ground motion recordings, the following experiment was performed. Using the RDP as a source for the elastic wave propagation code, the resulting wave field was propagated in a layered medium to receivers at appropriate distance ranges from the source.

The source-receiver geometry and the elastic structure in which they are embedded are shown in Figure 3.9. The information for this figure is from a report by Perret (1968). The receivers are at stations B-SL (range R = 201 m) and 16-SL (R = 470 m). Comparisons of the radial motions resulting
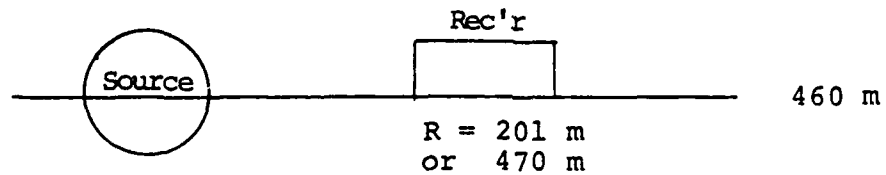
Figure 3.9. Piledriver elastic layering sonic-receiver geometry. Numbers in parentheses are P and S velocities (km/sec) and densities (gr./cm^3), respectively.

from calculations made using the structure in Figure 3.9 with
those using a homogeneous medium are shown in Figure 3.10.
Note that the free surface has a negligible effect on the
ground motion at B-SL, and a slightly greater effect at 16-SL
where the reflected ray is traveling more horizontally than
at B-SL. Also, the RVP's deduced from the radial velocities
in the above comparisons are shown to be nearly the same
(Figure 3.11). Thus, the assumption that the ground motion
recordings at these stations are unaffected by geologic layer-
ing seems warranted, and the waveforms observed for PILEDRIVER
were appropriate choices for normalizing the source calcula-
tions as described in Bache, et al. (1975b).

3.3   GASBUGGY SOURCE CALCULATION

3.3.1 Introduction

GASBUGGY, a nuclear experiment designed to stimulate
production of natural gas from the impervious Pictured Cliffs
sandstone formation, was detonated in Rio Arriba County, New
Mexico, in a layer of Lewis Shale (depth of burial of 4240
feet) approximately 40 feet below the Pictured Cliffs sand-
stone. The device yield was 29 kilotons. As part of this
experiment a program of free-field ground motion measure-
ments was carried out to define a seismic source function for
GASBUGGY. The set of ground motion measurements obtained
for GASBUGGY (Perret, 1972) provides an excellent oppor-
tunity to further verify the capability of the constitutive
modeling embodied in the SKIPPER code to predict close-in,
free-field ground motion from underground explosions. The
results of these types of calculations place important
constrains on the source spectra that are used for teleseis-
mic ground motion predictions.
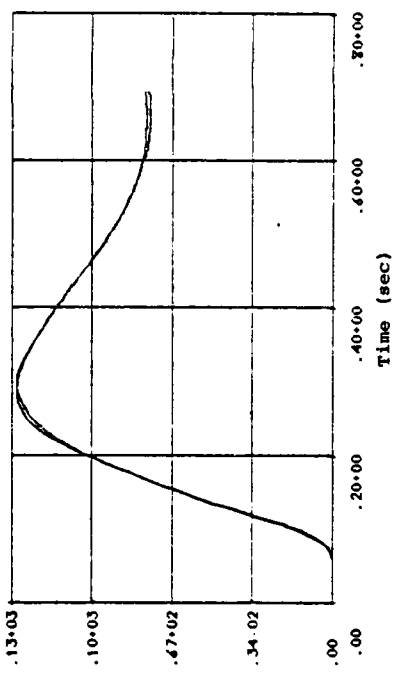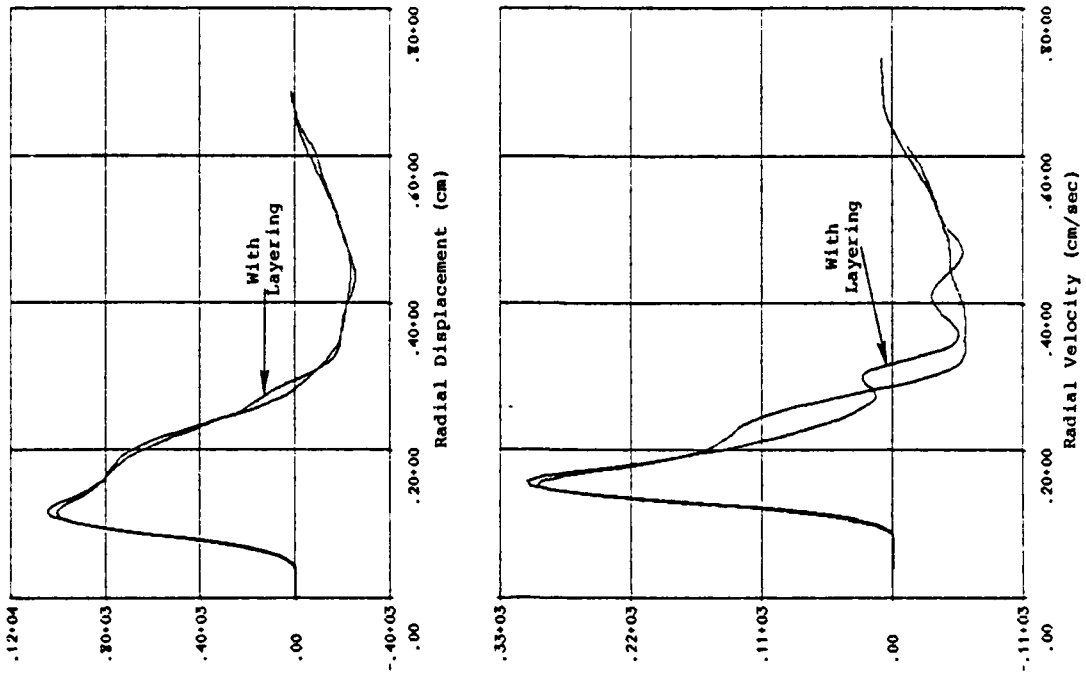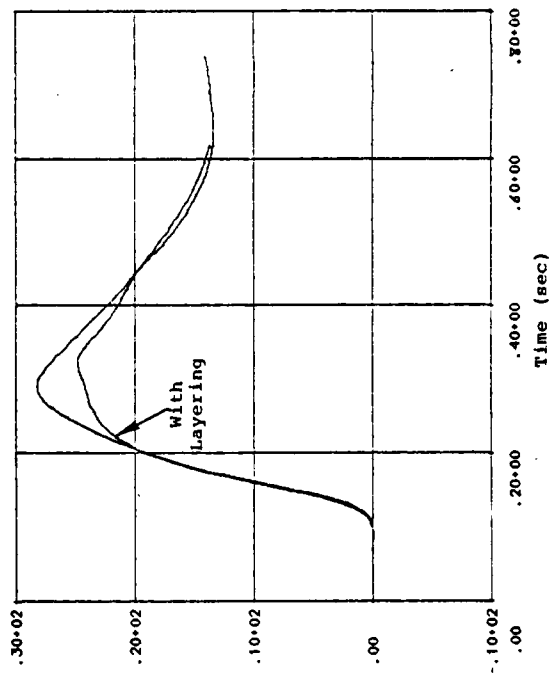
Figure 3.10. Comparison of radial motions using homogeneous and layered media.
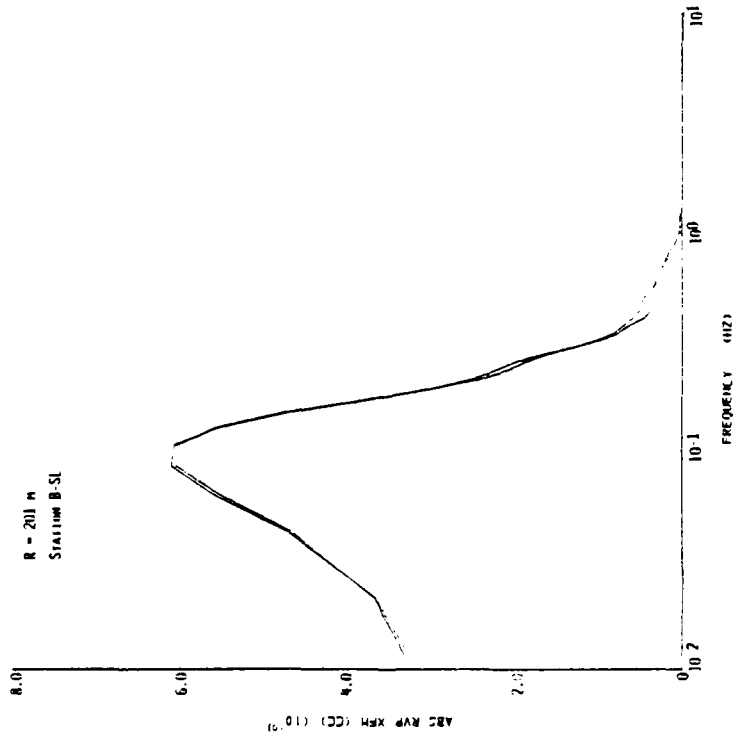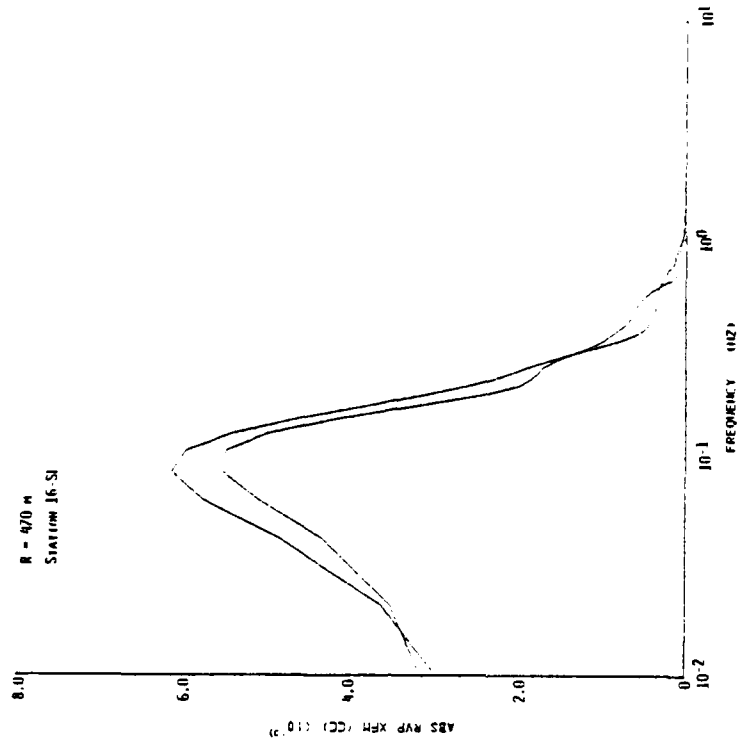
34

Figure 3.11. Amplitude spectra at two ranges comparing homogeneous and layered cases.

35

3.3.2 Source Calculation

Free-field instrumentation, consisting of three-component accelerometers and particle velocity gauges, was installed at four subsurface stations, located at slant ranges between approximately 1500 and 1900 feet from the GASBUGGY working point (Perret, 1972). Figure 3.12 shows both a plan view of the experimental arrangement (left) and a cross-sectional perspective of the subsurface station locations and local geologic layering.

Based on the free-field ground motion measurements, Perret (1972) computed the reduced displacement potential (RDP) for the GASBUGGY source at the four subsurface stations. The measured RDPs are shown in Figure 3.13. Although these four stations were located in different rock layers (Figure 3.11), the residual values of the RDPs are quite similar; differing from an average value of 6470 m^3 by at most 12.5 percent. Peak values of RDP at these stations also are relatively uniform. This indicates that the two dimensional effects of the layering on RDP are quite small. Therefore, the GASBUGGY environment was modeled by a spherically symmetric source calculation in an infinite layer of Lewis Shale.

Some material properties data for both Lewis Shale and Pictured Cliffs sandstone are available from Terhune and Shaw (1972). Figure 3.14 shows the failure envelopes for the materials of interest and Figure 3.15 the compressibility curves. A Tillotson equation of state was fitted to the compressibility curve for Lewis Shale. Other relevant material properties are given in Table 3.5. The constitutive modeling, tensile failure, effective stress law, etc. were the same as discussed for the KASSERI event.

Figure 3.16 shows the RDP obtained from a SKIPPER calculation using the above material properties. The RDP is in excellent agreement with the measured values of Figure 3.13.

TABLE 3.5

MATERIAL PROPERTIES FOR LEWIS SHALE

Bulk Density	2.48 gms/cm^3
Air-Filled Voids	0
Sonic Velocity	4.0 km/sec
Overburden Pressure	300 bars
Bulk Modulus	200 kbars
Shear Modulus	147.6 kbars

$$
\text{Failure Surface} \begin{cases} Y_0 & 0.2 \text{ kbars} \\ Y_m & 2.0 \text{ kbars} \\ \overline{P}_m & 7.0 \text{ kbars} \end{cases}
$$
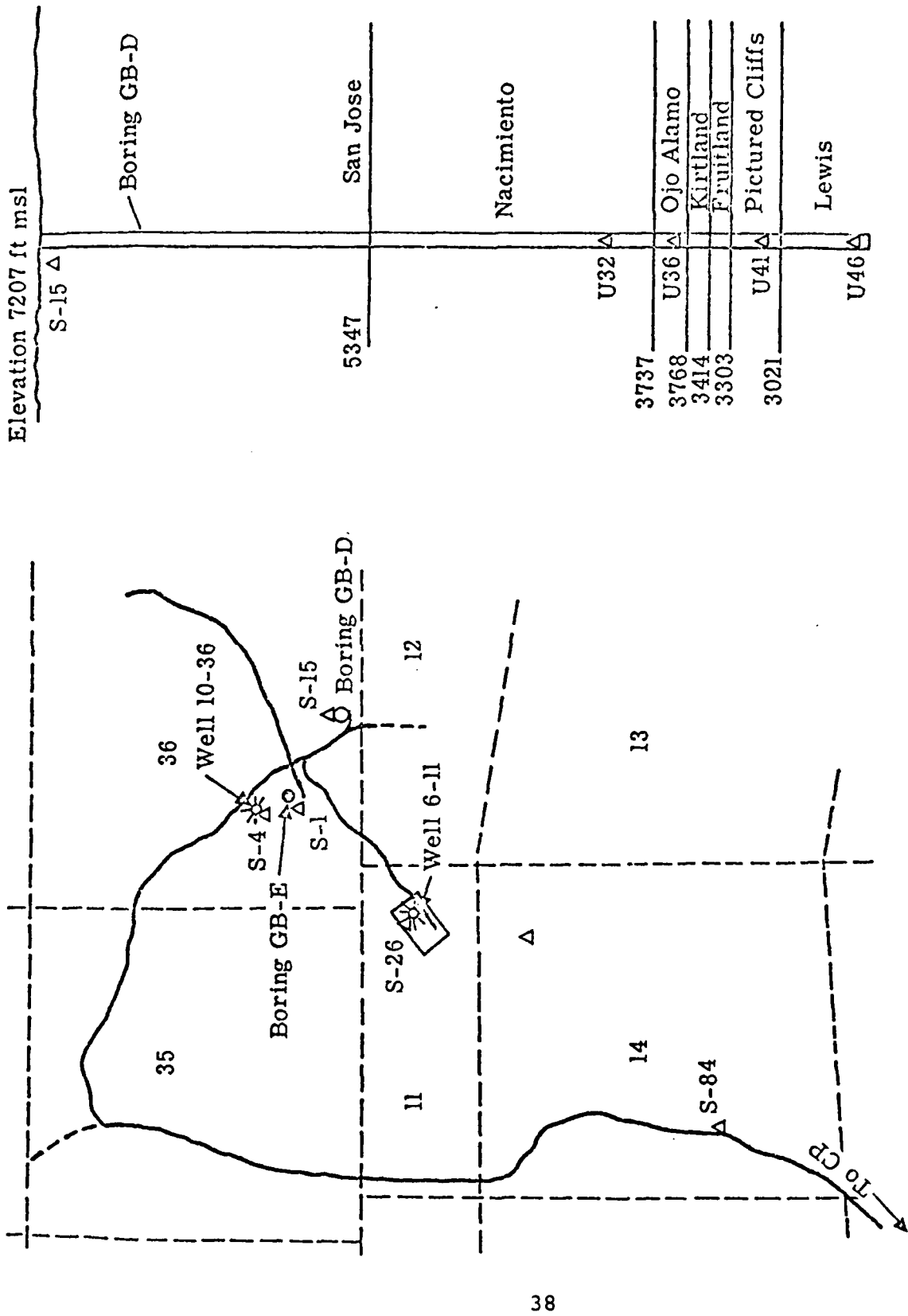
Subsurface Station Locations and Geology

Site Map

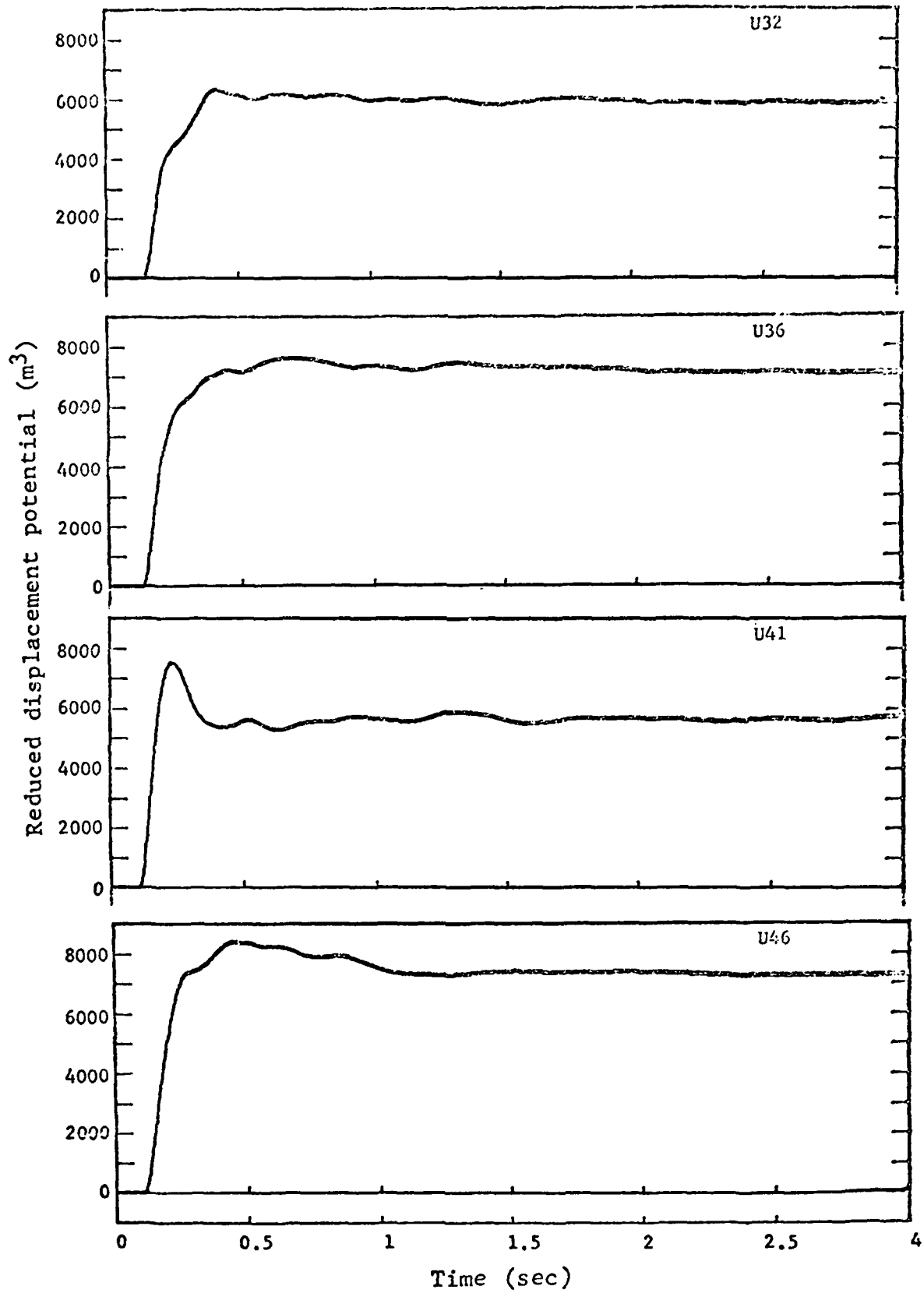Figure 3.12. Site map and instrument station locations.

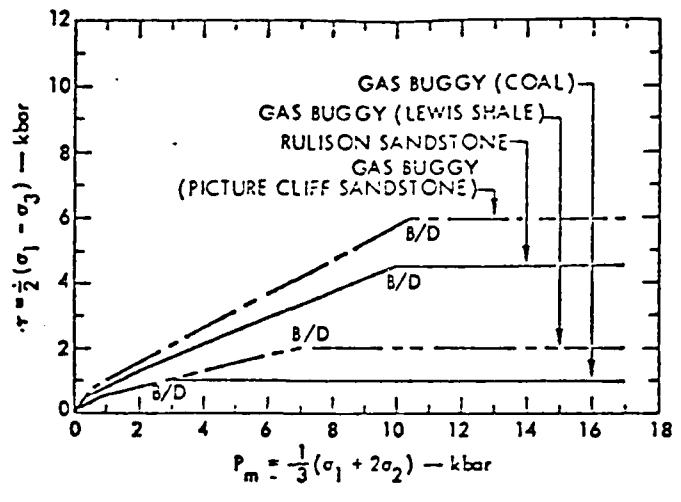Figure 3.13.   Reduced displacement potential records.

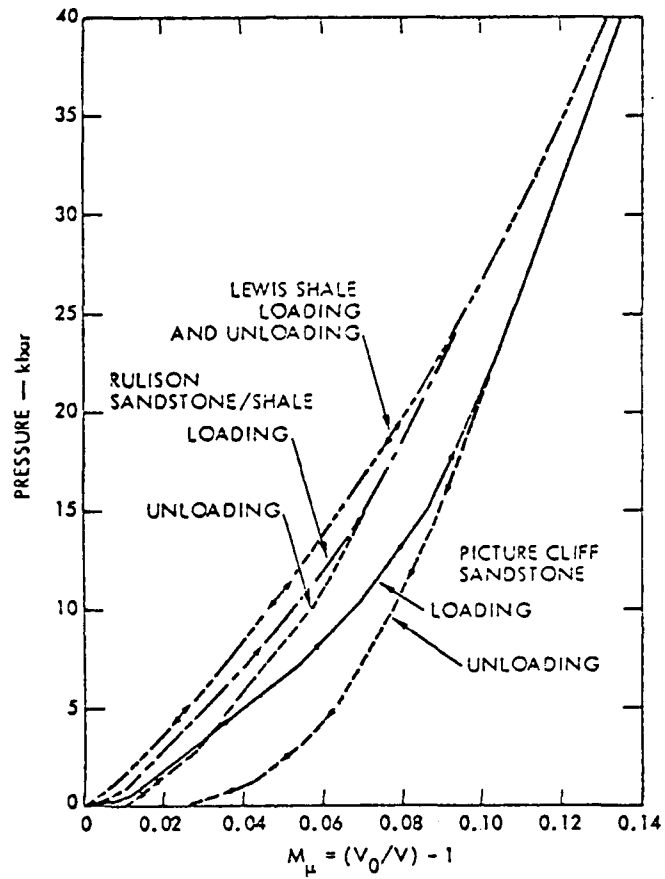Figure 3.14. Failure envelopes for GASBUGGY and RULISON.

Figure 3.15. Compressibility curves for RULISON and GASBUGGY.

GASBUGGY, LEWIS SHALE
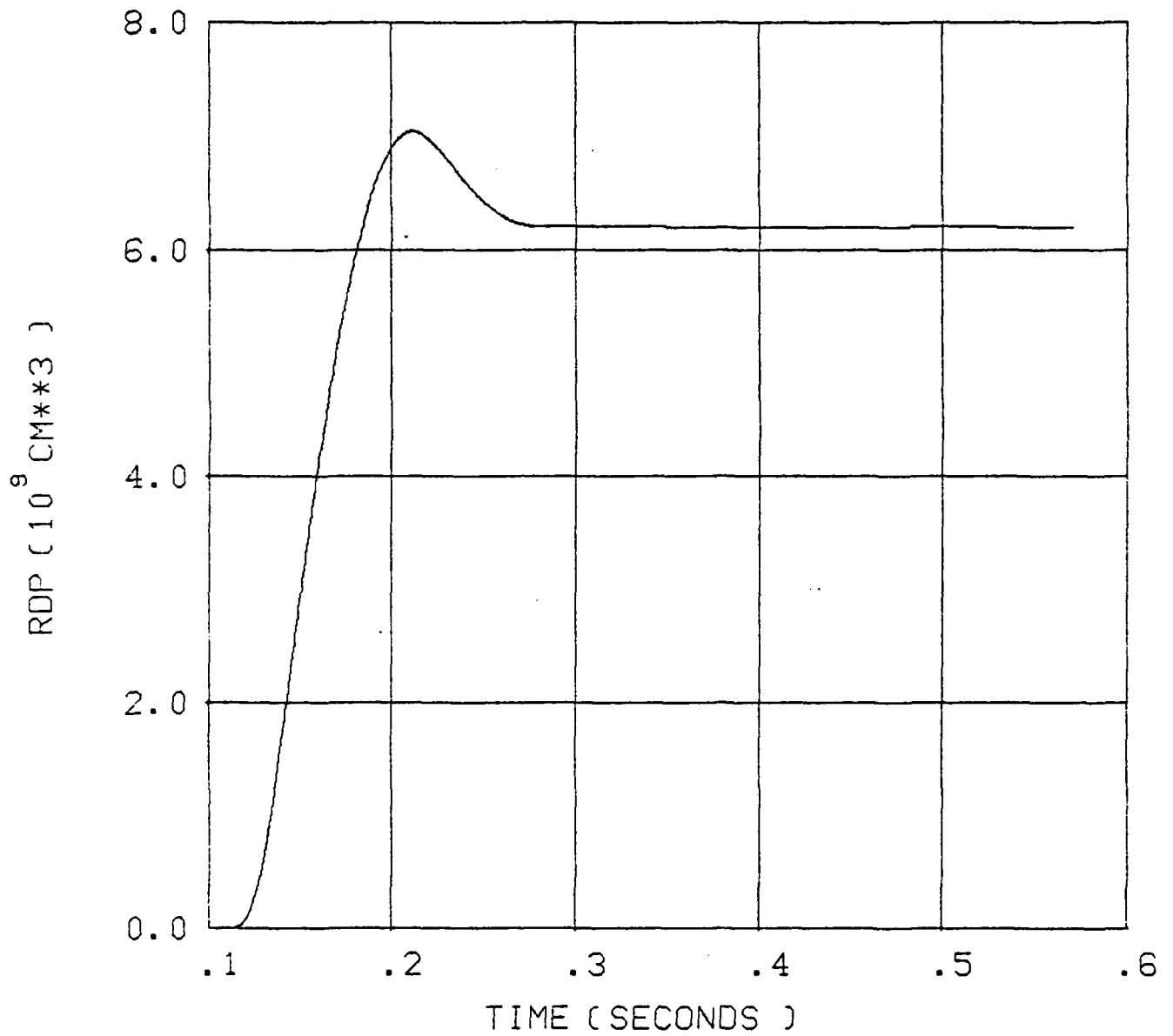

Figure 3.16.   GASBUGGY calculated RDP using material properties
for Lewis Shale.

Figure 3.17 shows the RDP obtained using Pictured Cliffs
sandstone material properties. The high strength of this
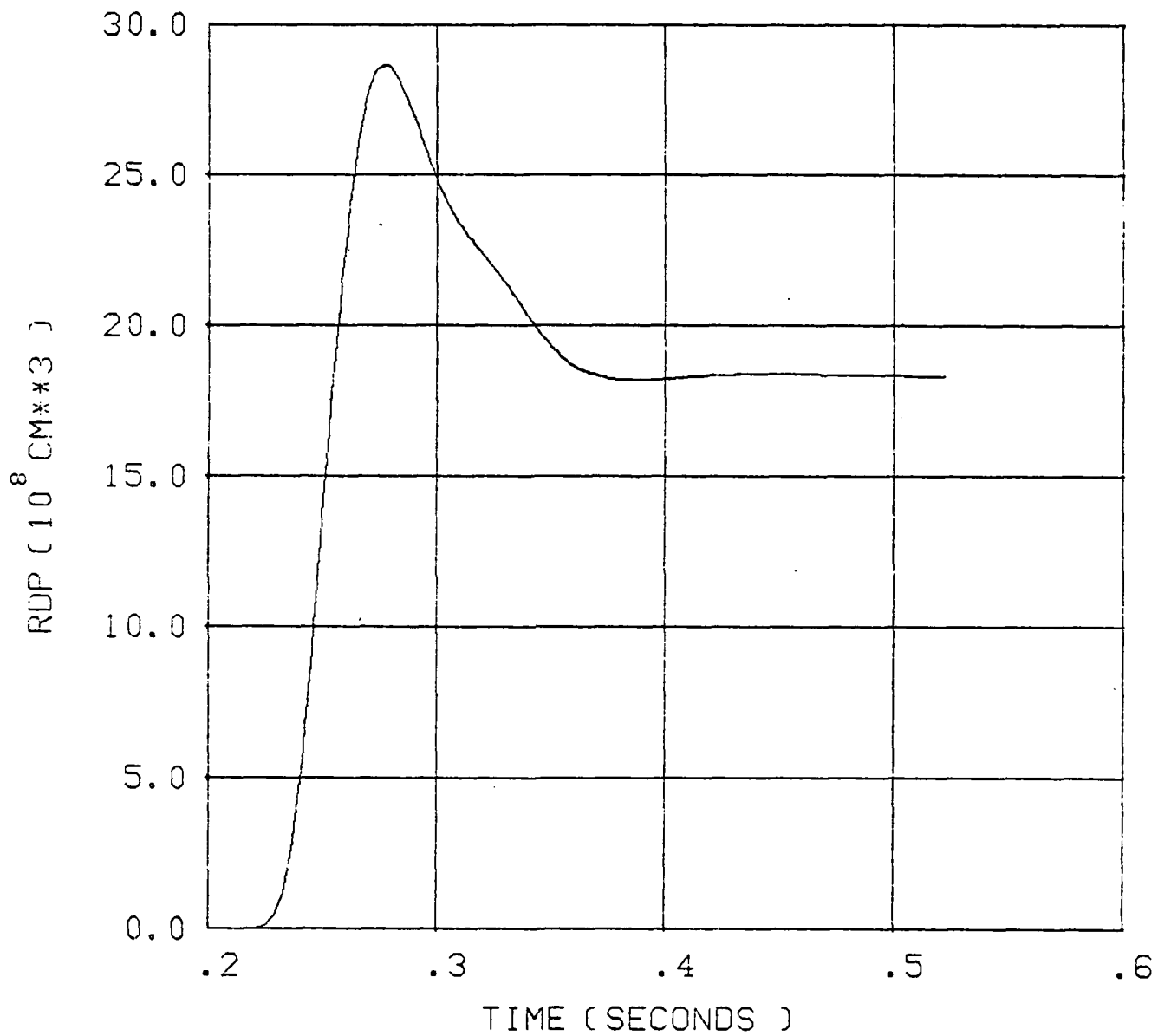rock results in an RDP much lower than measured.

GASBUGGY,PICTURE CLIFFS SANDSTONE

Figure 3.17.   GASBUGGY calculated RDP using material properties
               for Pictured Cliffs.

44

IV. CONCLUSIONS

Considerable progress was made during the fourth
three-month period of this project on several of the tasks
specified in the work statement of this contract.

The theoretically computed and observed amplitudes
of both the b and d (maximum) body wave phases for KASSERI
agree to well within a factor of two at all of the five
SDCS stations. Minor adjustments of the upper mantle model
could improve the agreement of all the SDCS sites.

Computations of the effect of material strength on
teleseismic body wave amplitudes indicate that the amplitude
of the b phase increases with decreasing strength; the rate
of increase being more rapid at lower levels of material
strength. An additional effect is that the apparent period
of the b phase increases rapidly with decreasing strength
due to a shift in the corner frequency of the source spectrum.

Further verification of the explosion source modeling
code, SKIPPER, was achieved by comparison of free field
ground motion calculations and observations for the PILEDRIVER
and GASBUGGY explosions. In the case of PILEDRIVER, the
exercise of a recently developed elastic wave propagation
code verified that the observed PILEDRIVER RDP was not af-
fected by reflected waves from the free surface or from layer
interfaces in the source region.

Excellent free field ground motion measurements and
material properties data are available for the GASBUGGY ex-
plosion. The computed RDP, employing these data, agrees quite
well with the measured RDP, increasing our confidence in the
constitutive modeling of the explosion source and ultimately
the teleseismic ground motion predictions based on these
source calculations.

V. REFERENCES

Bache, T. C., J. T. Cherry, K. G. Hamilton, J. F. Masso, and J. M. Savino (1975a), "Application of Advanced Methods for Identification and Detection of Nuclear Explosions from the Asian Continent," Systems, Science and Software Report SSS-R-75-2646, May.

Bache, T. C., J. T. Cherry, N. Rimer, J. M. Savino, T. R. Blake, T. G. Barker, and D. G. Lambert (1975b), "An Explanation of the Relative Amplitudes of the Teleseismic Body Waves Generated by Explosions in Different Test Areas at NTS," Systems, Science and Software Final Report for DNA, October.

Bache, T. C., and D. G. Harkrider (1976), "The Body Waves Due to a General Seismic Source in a Layered Earth Model: 1. Formulation of the Theory," to be submitted to the BSSA.

Barker, T. G., T. C. Bache, J. T. Cherry, N. Rimer, and J. M. Savino (1976), "Prediction and Matching of Teleseismic Ground Motion (Body and Surface Waves) from the NTS MAST Explosion," Systems, Science and Software Report SSS-R-76-2727 (Draft).

Cherry, J. T., N. Rimer, and W. O. Wray (1975), "Seismic Coupling from a Nuclear Explosion: The Dependence of the Reduced Displacement Potential on the Nonlinear Behavior of the Near Source Rock Environment," Systems, Science and Software Report SSS-R-76-2742, September.

Cherry, J. T., T. C. Bache, W. O. Wray, and J. F. Masso (1976), "Teleseismic Coupling from the Simultaneous Detonation of an Array of Nuclear Explosions," Systems, Science and Software Report SSS-R-76-2865.

Helmberger, D. V. (1968), "The Crust-Mantle Transition in the Bering Sea," BSSA, 58, 179-214.

Helmberger, D. V., and R. A. Wiggins (1971), "Upper Mantle Structure of the Midwestern United States," J. Geophys. Res., 76, 3229-3245.

Perret, W. R. (1968), "Free Field Ground Motions in Granite," Operation Flint Rock, Shot Piledriver, DASA POR-4001.

Perret, W. R. (1972), "Gasbuggy Seismic Source Measurements," Geophysics, 37, 301-312.

Riney, T. D., J. K. Dienes, G. A. Frazier, S. K. Garg, J. W. Kirsch, D. H. Brownell, and A. J. Good (1972), "Ground Motion Models and Computer Techniques," DNA-2915Z, Systems, Science and Software Report 3SR-1071.

Terhune, R. W., and J. G. Shaw (1972), "Calculation of Rock Fracturing from Multipel Nuclear Explosive Sources," Lawrence Livermore Laboratory Report UCRL-74017, October 31.

APPENDIX A

EFFECT OF INSTRUMENT RESPONSE ON MEASURED AMPLITUDES

Standard procedure for determining ground motion amplitudes from seismograph recordings requires correction for the instrument response at the apparent period of the cycle being measured. There are several possible sources of error in this procedure:

1. The signal is not monochromatic and a single period correction factor can never entirely remove the instrument effect.

2. The amplitude and phase response of the instrument at the time the signal is recorded may not be accurately known.

3. It is often difficult to accurately measure the dominant period of the cycle being measured.

These are all sources of error that refer to a single recording by a single instrument. While everyone knows they exist, a quantitative estimate of their effect is not so widely known.

If we are comparing measured amplitudes from a series of events that have similar waveforms and are recorded by the same (nominal) instrument, then the errors 1 - 3 listed above should be normally distributed and can be accounted for by statistical methods. Let us here pose a different question. Assume that the same ground motion is recorded by a number of different instruments and that the measurements are accurately made. After correcting for the instrument response at the apparent period of the cycle being measured, how closely do the estimates of ground motion agree? In this appendix we give the results of several numerical experiments that indicate that the differences can be surprisingly large.

First, let us consider the effect on body wave measurements. The instruments to be discussed are as follows. For the standard of comparison let us take the LRSM Benioff short period instrument for which nominal response curves were given in all the old SDAC shot reports. We have been interested in computing the ground motion at five SDAC stations, RKON, CPSO, WHY2K, FNWV, HNME. Calibration data from June 12, 1975 was supplied by the project officer for each of these stations. This was in the form of $\approx$ 5 amplitude response values and a series of phase response values. The data were not entirely consistent and had to be smoothed. Certainly, it is valid to ask how trustworthy these calibration data are, but it is the best we have.

Let us view the same explosion-like ground motion through the six instruments which we denote as LRSM and by the names of the five SDCS stations. The ground motion is that computed for KASSERI at HNME with $T/Q = 1.05$. The resulting seismograms are shown in Figure A.1. In terms of signal shape, the main difference is that distinguishing the LRSM record from the other five. We also notice that the 1 Hz peak amplitude values given with each record vary over a substantial range (1.02 - 1.36 μ) with the LRSM record again being exceptional.

What are the amplitudes associated with the seismograms of Figure A.1? With these theoretical records we can reduce the measurement errors to nearly vanishing. Rather than measuring by eye, a parabola is fit to the digital data defining the peaks. The amplitude and apparent period of the cycle of interest can then be determined with sources of human error removed. Since the instrument is input to the code in digital form, we can determine the (theoretical) instrument response at the apparent period with essentially zero error. The amplitude and period data for the b and
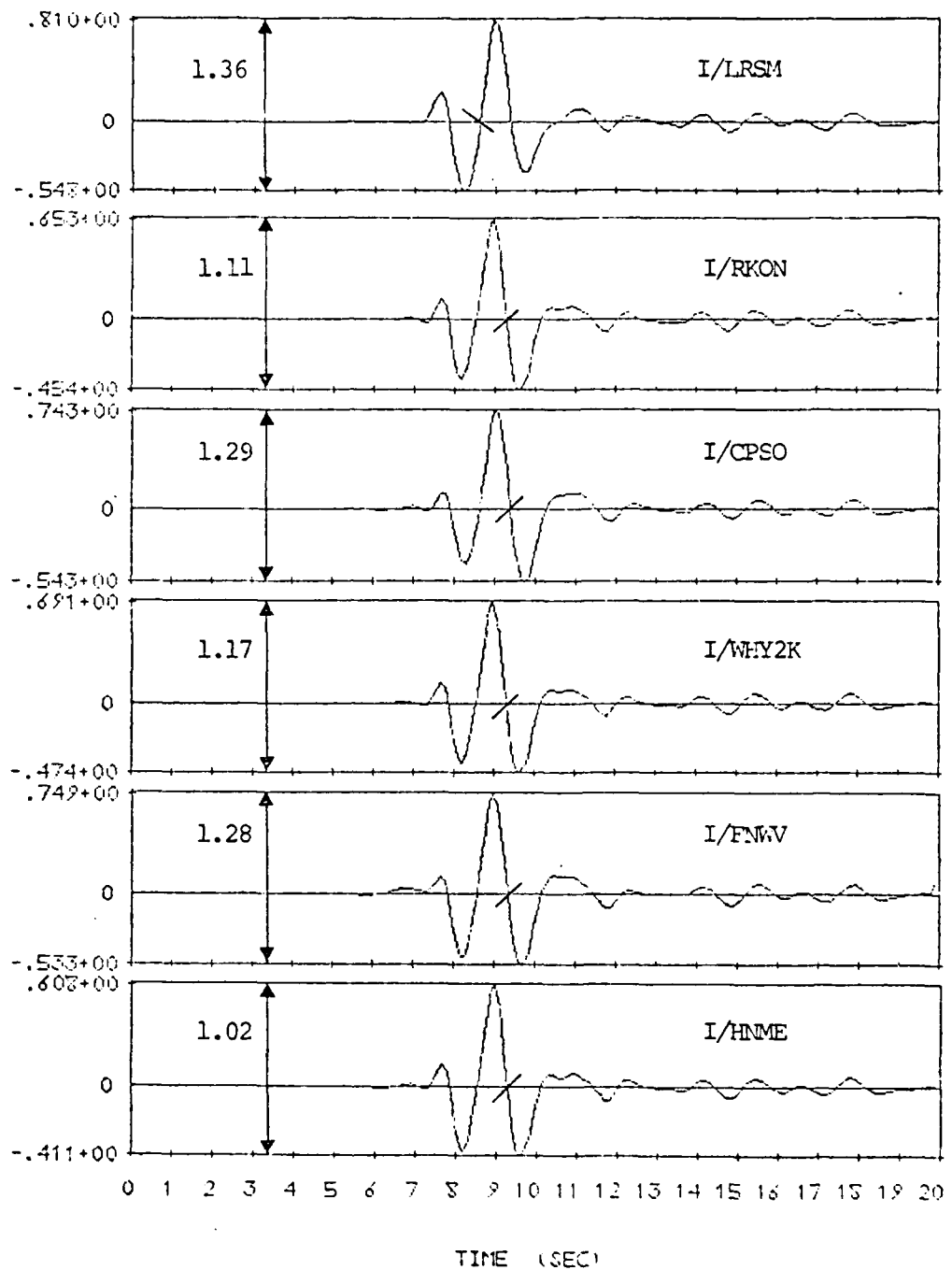
Figure A.1. Theoretical ground motion for KASSERI at HNME as
viewed with six different instruments. The in-
strument designations appear on each seismogram
as I/name. For the calculations T/Q = 1.05.

d phases is summarized in Table A.1. The maximum or d phase
is indicated on the seismograms by a bar.

Table A.1. Amplitude and Period Data for the Records of
Figure A.1

Instrument	T_b	b (mµ)	T_d	d (mµ)
I/LRSM	1.16	1079	1.52	3373
I/RKON	0.97	493	1.35	2589
I/CPSO	1.05	607	1.43	3093
I/WHY2K	0.99	537	1.37	2670
I/FNWV	1.06	686	1.39	2725
I/HNME	0.97	491	1.`2	2390

The amplitude and period differences are startling.
If we just consider the SDCS instruments, the period varies
by 0.1 second and the amplitude by ≈ 40 percent. However,
the LRSM gives an amplitude that can differ by more than a
factor of two! Unfortunately, the instrument correction
acts in the wrong way. If we were to make no instrument
correction other than to the gain at 1 Hz, the discrepancy
in amplitudes in the data of Table A.1 would be much reduced.
For example, with no correction the b amplitudes for the
SDCS instruments vary from 523 - 695 mµ and the LRSM ampli-
tude is 783 mµ. Perhaps we should not make instrument cor-
rections!

What about when the actual ground motion is different
from that used in the comparison above? Let us consider
KASSERI as computed at each of the SDCS stations with earth
model HWNE-3 and T/Q = 1.05. We compute seismograms at each
of the stations, first with the LRSM nominal instrument,
then the instrument response specific to each station. The

results are shown in Figure A.2 and the amplitudes are summarized in Table A.2.

Table A.2.   Amplitude and Period Data for the Records of
             Figure A.2

Station	Instrument	T_b	b	T_d	d
RKON	LRSM Nominal	1.09	2682	1.48	9345
	Specific	0.95	1337	1.35	2589
CPSO	LRSM Nominal	1.29	2061	1.84	6986
	Specific	1.17	1249	1.43	3093
WHY2K	LRSM Nominal	1.19	646	1.38	4452
	Specific	1.03	336	1.37	2670
FNWV	LRSM Nominal	1.43	1078	1.49	2024
	Specific	1.38	732	1.34	2725
HNME	LRSM Nominal	1.16	1079	1.52	3373
	Specific	0.97	491	1.32	2390

In Table A.3 we show the same kind of comparison for ground motion from the MAST event. In this case the dominant period of the actual ground motion is somewhat shorter than for KASSERI. Only the data for the b amplitude is shown as it illustrates our point — the instrument response can make a big difference in the apparent ground motion determined from seismograms by conventional means.
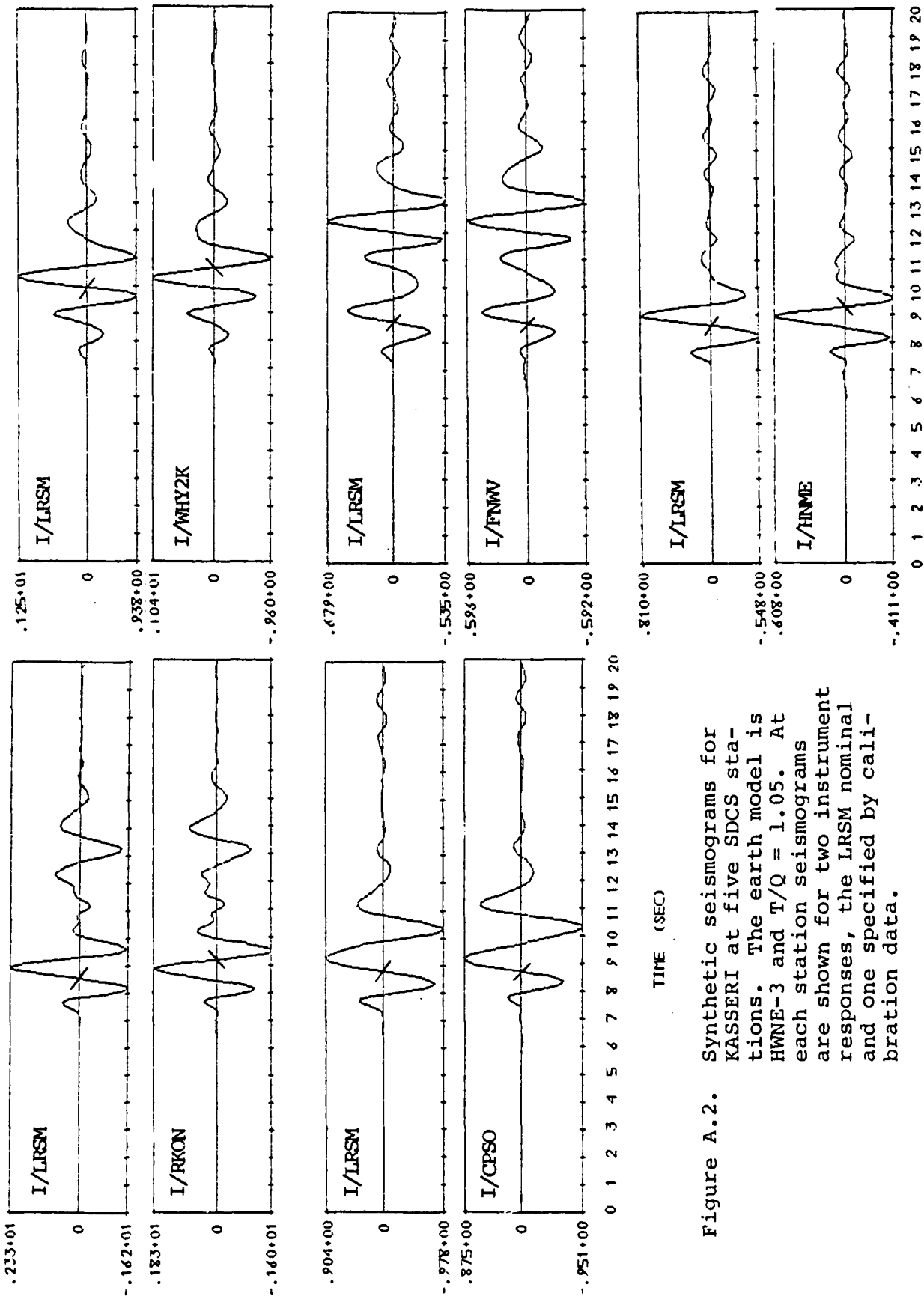
Figure A.2. Synthetic seismograms for KASSERI at five SDCS stations. The earth model is HWNE-3 and T/Q = 1.05. At each station seismograms are shown for two instrument responses, the LRSM nominal and one specified by calibration data.

53

Table A.3. Amplitude and Period Data for MAST Seismograms
Computed with the LRSM Nominal and Station
Specific Instruments

Station	Instrument	T_b	b
RKON	LRSM Nominal	0.93	1154
	Specific	0.86	775
CPSO	LRSM Nominal	0.94	603
	Specific	0.92	478
WHY2K	LRSM Nominal	0.94	237
	Specific	0.89	167
FNWV	LRSM Nominal	1.08	248
	Specific	1.02	168
HNME	LRSM Nominal	0.93	415
	Specific	0.86	270